nature communications

Article

https://doi.org/10.1038/s41467-025-57962-9

FoxO3 controls cardiomyocyte proliferation and heart regeneration by regulating Sfrp2 expression in postnatal mice

Received: 20 May 2024

Accepted: 7 March 2025

Published online: 14 March 2025

Check for updates

Jing-Bo Xia[1,2,9], Kun Liu[1,3,9], Xiao-Lin Lin[1,9], Hong-Ji Li[1,9], Jin-Hua Lin[1], Li Li[4], Chi-Qian Liang[1], Yan Cao[1], Na Wen[1], Zhao-Fu Liao[5], Hui Zhao[6], Kyu-Sang Park[7], Guo-Hua Song[8], Ze-Bing Ye[2] ✉, Dong-Qing Cai[1] ✉, Zhen-Yu Ju[1] ✉ & Xu-Feng Qi[1,2] ✉

The Forkhead box O3 (FoxO3) transcription factor is crucial to controlling heart growth in adulthood, but its exact role in cardiac repair and regeneration in postnatal mice remains unclear. Here, we show that FoxO3 deficiency promotes cardiomyocyte proliferation in postnatal mice and improves cardiac function in homeostatic adult mice. Moreover, FoxO3 deficiency accelerates heart regeneration following injury in postnatal mice at the regenerative and non-regenerative stages. We reveal that FoxO3 directly promotes the expression of secreted frizzled-related protein 2 (Sfrp2) and suppresses the activation of canonical Wnt/β-catenin signaling during heart regeneration. The increased activation of β-catenin in FoxO3-deficient cardiomyocytes can be blocked by Sfrp2 overexpression. In addition, Sfrp2 overexpression suppressed cardiomyocyte proliferation and heart regeneration in FoxO3-deficient mice. These findings suggest that FoxO3 negatively controls cardiomyocyte proliferation and heart regeneration in postnatal mice at least in part by promoting Sfrp2 expression, which leading to the inactivation of canonical Wnt/β-catenin signaling.

In the past several decades, it was widely believed that mammalian heart is a terminally differentiated organ, which is incapable of regenerating after injury during adult period. Although recent studies revealed that limited myocyte turnover occurs in the adult mammalian heart, it is insufficient to restore contractile function after cardiac injury[1–4]. Therefore, a scientific and clinical imperative is to identify targets involved in the regulation of regenerative capacity in mammalian hearts[5,6]. Most cardiomyocytes exit the cell cycle and continue to grow in size after the first week of postnatal life in mice[7,8], which results in limited regenerative capacity in adult period[1,4]. However, adult hearts of lower vertebrates such as zebrafish and amphibians have a robust regenerative response to injury[9–12]. It has also been evidenced that completely cardiac regeneration occurs in postnatal mouse heart during the first week of postnatal life, but this capacity

[1]Key Laboratory of Regenerative Medicine of Ministry of Education, Institute of Aging and Regenerative Medicine, Department of Developmental & Regenerative Biology, College of Life Science and Technology, Jinan University, Guangzhou 510632, China. [2]Department of Cardiology, The Affiliated Guangdong Second Provincial General Hospital, Jinan University, Guangzhou 510317, China. [3]Department of Cardiology, Zhongshan Torch Development Zone People's Hospital, Zhongshan 528437, China. [4]Department of Cardiology, Guangzhou Red Cross Hospital, Jinan University, Guangzhou 510220, China. [5]Guangdong Provincial Key Laboratory of Medical Molecular Diagnostics, Guangdong Medical University, Dongguan 523808, China. [6]Key Laboratory of Regenerative Medicine of Ministry of Education, School of Biomedical Sciences, Faculty of Medicine, The Chinese University of Hong Kong, Hong Kong SAR, China. [7]Department of Physiology, Wonju College of Medicine, Yonsei University, Wonju, Gangwon 220-701, Korea. [8]School of Basic Medical Sciences, Shandong First Medical University & Shandong Academy of Medical Science, Jinan 250117, China. [9]These authors contributed equally: Jing-Bo Xia, Kun Liu, Xiao-Lin Lin, Hong-Ji Li. ✉e-mail: bean9350@sina.com; tdongbme@jnu.edu.cn; zhenyuju2016@jnu.edu.cn; qixufeng@jnu.edu.cn

markedly diminishes by postnatal day 7 (p7)[13,14]. Based on previous reports, it is believed that cardiac regeneration in postnatal mice[13–16], as well as in adult zebrafish[9,10] and amphibians[11,12,17], is primarily mediated by cardiomyocyte proliferation. Therefore, it is crucial to explore relative signaling networks and the underlying molecular mechanism responsible for postnatal cardiomyocyte proliferation.

FoxO transcription factors belong to the Forkhead family of transcriptional regulators, and play important roles in cell proliferation, metabolism, and aging in a variety of cell types[18–22]. Although four FoxO isoforms (FoxO1, FoxO3, FoxO4, and FoxO6) have been identified in mammals, the loss-of-function mutation of individual FoxO isoforms results in specific phenotypes, indicating the different roles for each FoxO isoform[23]. Among the four isoforms, FoxO1 and FoxO3 show a high expression level in developing and adult hearts[18,24,25]. Combined deletion of FoxO1 and FoxO3 specifically in cardiomyocytes results in increased cardiac injury following acute ischemia and reperfusion in adult mice[24]. Although both global overexpression and knockout of FoxO1 causes embryonic lethality of mice at E10.5, the cardiomyocyte-specific expression of constitutively active form of FoxO1 (caFoxO1) suppresses cardiomyocyte proliferation through activation of cell cycle inhibitor genes[18,23]. However, mice globally lacking FoxO3 are viable and enhance calcineurin signaling as well as cardiac growth in adulthood, suggesting the growth-regulating effect of FoxO3[23,26]. Consistently, using a mouse model of cardiomyocyte-specific overexpression of a constitutively active form of FoxO3 (caFoxO3), it was demonstrated that forced expression of FoxO3 induces cardiac atrophy, but fails to suppress cardiac hypertrophy induced by transverse aortic constriction[27]. These studies suggest that physiological levels of FoxO3 play an important role in the regulation of heart growth and cardiac function in adult mice.

The increasing knowledge about the crucial roles of FoxO3 in cultured cardiomyocytes and murine heart tissues[18,24,27], suggest the clinical signification of FoxO3 in cardiac disease[25,28]. However, the role of FoxO3 in the regenerative capacity of postnatal heart remains unclear. Moreover, it is not yet clear whether FoxO3-mediated biological function in postnatal heart influences adult heart growth and function. We found that FoxO3 activity is decreased during postnatal heart regeneration upon injury, which is correlated with an increase in cardiomyocyte proliferation as well as decrease of negative regulators of proliferation and cell cycle. Our data from loss-of-function genetic experiments demonstrate that FoxO3 knockout promotes cardiomyocyte proliferation and heart regeneration in postnatal mice at regenerative and non-regenerative stages, at least in part, through downregulating Sfrp2 and subsequently activating the canonical Wnt/β-catenin signaling. We propose that FoxO3 is required to control cardiomyocyte proliferation during heart regeneration in postnatal mice.

Results

FoxO3 expression profile in postnatal and injured hearts

It has been demonstrated that cardiac regeneration can occur in neonatal mouse following an injury produced in the first week of life[13,14]. This prompts us to ask the expression patterns of FoxO3 in mouse heart after birth. To determine the expression and localization of FoxO3 in cardiomyocytes, primary cardiomyocytes isolated from neonatal mice at postnatal day 1 (p1) were subjected to immunofluorescent staining. Z-stack confocal microscopy analysis revealed that FoxO3 was predominantly expressed in the nuclei of cardiomyocytes (Supplementary Fig. 1a, b). Consistent with the observation in primary cardiomyocytes, FoxO3 was also dominantly detected in the nuclei of cardiomyocytes in hearts from postnatal mice (Supplementary Fig. 1c). Moreover, FoxO3 expression levels significantly increases with the heart growth from neonatal (p1) to adult (p84) stages (Supplementary Fig. 1d). Although FoxO3 dramatically expressed in the nuclei of cardiomyocytes, little FoxO3 expression was also detected in the non-cardiomyocytes as indicated by arrowhead in Supplementary Fig. 1a. To further explore FoxO3 expression patterns in cardiomyocytes (CMs) and non-cardiomyocytes (nCMs) during heart maturation, primary CMs and nCMs were isolated from postnatal mice at p1 and p56, respectively. The qPCR assay revealed that FoxO3 mRNA expression levels were significantly increased in adult CMs and nCMs when compared with neonatal ones, respectively (Supplementary Fig. 1e).

To determine the response of FoxO3 to heart injury, we resected ventricular apex of neonatal heart at p1 and examined the expression of FoxO3 protein at 1 day post-resection (1 dpr) and 5 dpr, respectively. Western blotting analysis showed that heart injury significantly increased the phosphorylation of FoxO3 on Thr 32 and Ser 253 (Fig. 1a-d), indicating the decreased activation of FoxO3. Immunofluorescence staining further revealed that both expression level of FoxO3 and percentage of FoxO3-positive cardiomyocytes in apical and remote zone were significantly decreased at 5 dpr when compared with sham group (Fig. 1e-j). Consistently, western blotting further confirmed the reduction of FoxO3 in the primary cardiomyocytes isolated from the injured hearts at 5 dpr compared with sham group (Fig. 1k). These data suggest that FoxO3 activation decreases in neonatal heart upon injury. It's well known that Akt is an upstream negative mediator of FoxO3 that can promote the phosphorylation of FoxO3, thereby suppressing its activation[29]. To further explore the molecular mechanisms regulating FoxO3 activation during neonatal heart injury, we examined the activation of Akt pathway and found that the Akt phosphorylation level was significantly increased in the injured heart at 5 dpr (Fig. 1l). These findings suggest that Akt-mediated inactivation of FoxO3 might play an important role in heart regeneration.

In vitro effects of FoxO3 on cardiomyocyte proliferation

To elucidate the potential role of FoxO3 in cardiomyocyte proliferation in vitro, the siRNA targeting FoxO3 (siFoxO3) and negative control (siNC) were used to treat the primary cardiomyocytes isolated from neonatal mice at p1. The silencing efficiency of siFoxO3 was confirmed at both mRNA and protein levels (Supplementary Fig. 2a, b). Firstly, the cell cycle entry of cardiomyocytes was evaluated by measuring the nuclear incorporation of 5-ethynyl-2′-deoxyuridine (EdU), an efficient marker of DNA synthesis. As shown in Supplementary Fig. 2c, the representative EdU incorporation in cardiomyocytes was captured by confocal microscopy in both siNC- and siFoxO3-treated groups. However, quantification revealed that the percentage of EdU^+ $cTnT^+$ cells significantly increased in siFoxO3-treated group compared with control group (Supplementary Fig. 2d). Consistent with these findings, Ki67 and cTnT double staining revealed that FoxO3 knockdown leads to an increase in the percentage of $Ki67^+$ $cTnT^+$ cells, indicating an elevated proliferation level of primary cardiomyocytes (Supplementary Fig. 2e, f). To prove complete cardiomyocyte proliferation, late cell cycle markers including phospho-Histone H3 (pH3) and aurora kinase B (AurkB) were further used in this study. Consistently, the percentage of $pH3^+$ $cTnT^+$ cells was significantly elevated by FoxO3 knockdown (Supplementary Fig. 2g, h), indicating that FoxO3 knockdown really promotes the complete proliferation of cardiomyocytes in vitro. Importantly, increased percentage of $AurkB^+$ cardiomyocytes was also detected in the siFoxO3-treated group compared with control group (Supplementary Fig. 2i, j), implying the increased cytokinesis of cardiomyocytes. Consistent with these results from primary cardiomyocytes, increased proliferation was also detected in the siFoxO3-treated HL-1 cardiomyocytes compared with control cells (Supplementary Fig. 2k–m). These findings from primary cardiomyocytes and cell line strongly demonstrated that FoxO3 might negatively control cardiomyocyte proliferation.

FoxO3 knockout promotes cardiomyocyte proliferation in postnatal mice

To elucidate the potential role of FoxO3 in cardiomyocyte proliferation in postnatal heart, a cardiomyocyte-specific knockout mouse

https://doi.org/10.1038/s41467-025-57962-9

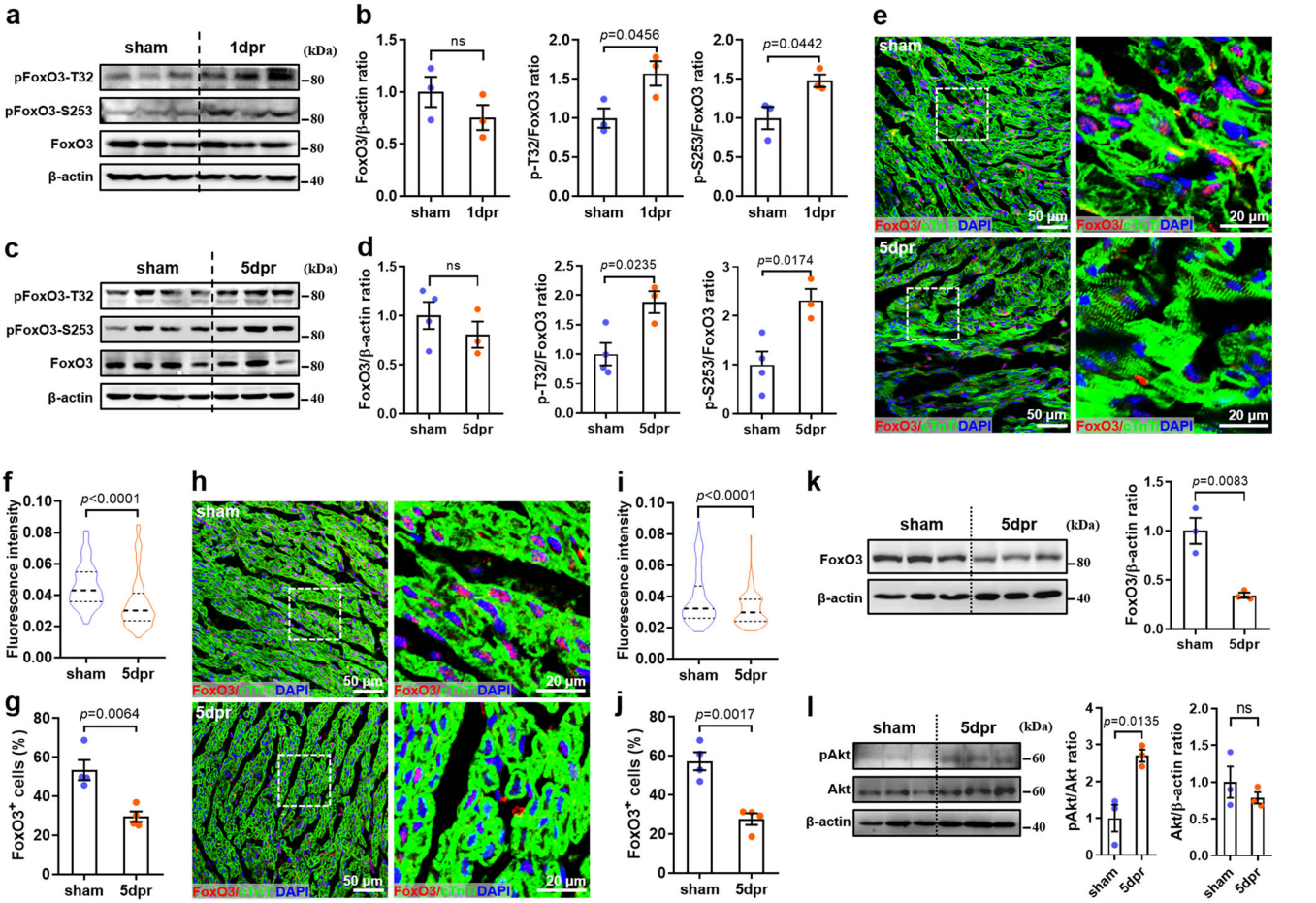

Fig. 1 | FoxO3 activation decreases upon heart injury in postnatal heart. Apical resection was performed at postnatal mice at p1, followed by sample collection at 1 dpr and 5 dpr, respectively. **a**, **b** Representative images (**a**) and quantification (**b**) of western blotting for FoxO3 expression and its phosphorylation in postnatal heart at 1 dpr ($n = 3$ hearts per group). (**c**, **d** Representative images (**c**) and quantification (**d**) of western blotting for FoxO3 expression and its phosphorylation in postnatal heart at 5 dpr ($n = 4$ hearts for sham and 3 hearts for 5 dpr). **e**–**g** Representative images (**e**) and quantification of FoxO3 fluorescent intensity (**f**, ~400 cells in 4 hearts per group) and FoxO3-positive cells (**g**, $n = 4$ hearts per group) in apical zone at 5 dpr. **h**–**j** Representative images (**h**) and quantification of FoxO3 fluorescent intensity (**i**, n = ~400 cells per group) and FoxO3-positive cells (**j**, $n = 4$ hearts per group) in remote zone at 5 dpr. **k** Western blotting validation of FoxO3 in primary cardiomyocytes isolated from hearts at 5 dpr ($n = 3$ per group). **l** Representative images (left) and quantification (right) of western blotting for Akt expression and its phosphorylation in postnatal heart at 5 dpr ($n = 3$ hearts per group). All data are presented as the mean ± SEM. *P* values are from two-tailed *t* test. ns, no significant difference. Source data are provided as a Source data file.

model (CKO) was generated by intercrossing *FoxO3*-floxed ($FoxO3^{fl/fl}$) mice[21] with Myh6-Cre transgenic mice (Supplementary Fig. 3a). Cardiac-specific deletion of FoxO3 in CKO mice were determined in protein and mRNA levels (Supplementary Fig. 3b–d). To determine whether FoxO3 knockout influences heart growth in postnatal mice, heart weight (HW) to tibial length (TL) ratio (HW/TL) was analyzed at p1 and p14. The increased HW/TL ratio were detected in CKO mice at p14 (Fig. 2a), indicating that FoxO3 knockout might promote postnatal heart growth. This idea was further confirmed by the morphological (Fig. 2b) and histological (Fig. 2c) analysis of hearts from CKO and Con mice at p1 and p14. To explore whether the FoxO3 knockout-induced heart growth results from myocardial hypertrophy, we further assessed cardiomyocyte size at p14 with wheat germ agglutinin (WGA) staining. Surprisingly, cardiomyocyte size was smaller in CKO hearts at p14 compared to controls (Fig. 2d). Moreover, there were not significant increases in the expression of myocardial hypertrophy markers including ANP, BNP, and Myh7 in the CKO hearts at p1 and p14 compared with controls (Supplementary Fig. 4). These results imply that cardiomyocyte number might be increased in the FoxO3-deficient hearts. To confirm this idea, we quantified the cardiomyocytes isolated from CKO and Con hearts at p14, and revealed a significant increase in the total number of cardiomyocytes in CKO hearts compared with controls (Fig. 2e). Consistent with this result, an increase in mononucleated cardiomyocytes and a decrease in binucleated cardiomyocytes were observed in CKO hearts compared with controls (Fig. 2f), which reflecting the proliferation or mitosis of cardiomyocytes as previously demonstrated[15,30]. These findings suggest that cardiomyocyte-specific knockout of FoxO3 might promote postnatal heart growth through increasing cardiomyocyte proliferation.

To further confirm this conjecture, hearts from CKO and Con postnatal mice at p1 and p14 were then subjected to immunofluorescent staining to evaluate cardiomyocyte proliferation. We firstly examined EdU incorporation and found that the percentage of EdU^+ $cTnT^+$ cells was significantly higher in CKO mice at p1 and p14 than that in Con mice, respectively (Fig. 2g). We subsequently quantified the number of cardiomyocytes that were positive for the mitosis marker pH3, and found that there was a significant increase in $pH3^+$ cardiomyocytes in CKO mice at p1 and p14 compared with controls (Fig. 2h), suggesting that FoxO3 knockout really promotes the complete proliferation of cardiomyocytes in postnatal mice. In addition, proliferating cardiomyocytes at p7, a time point just beyond the regenerative windows of neonatal heart, were confirmed by proliferating cell nuclear

https://doi.org/10.1038/s41467-025-57962-9

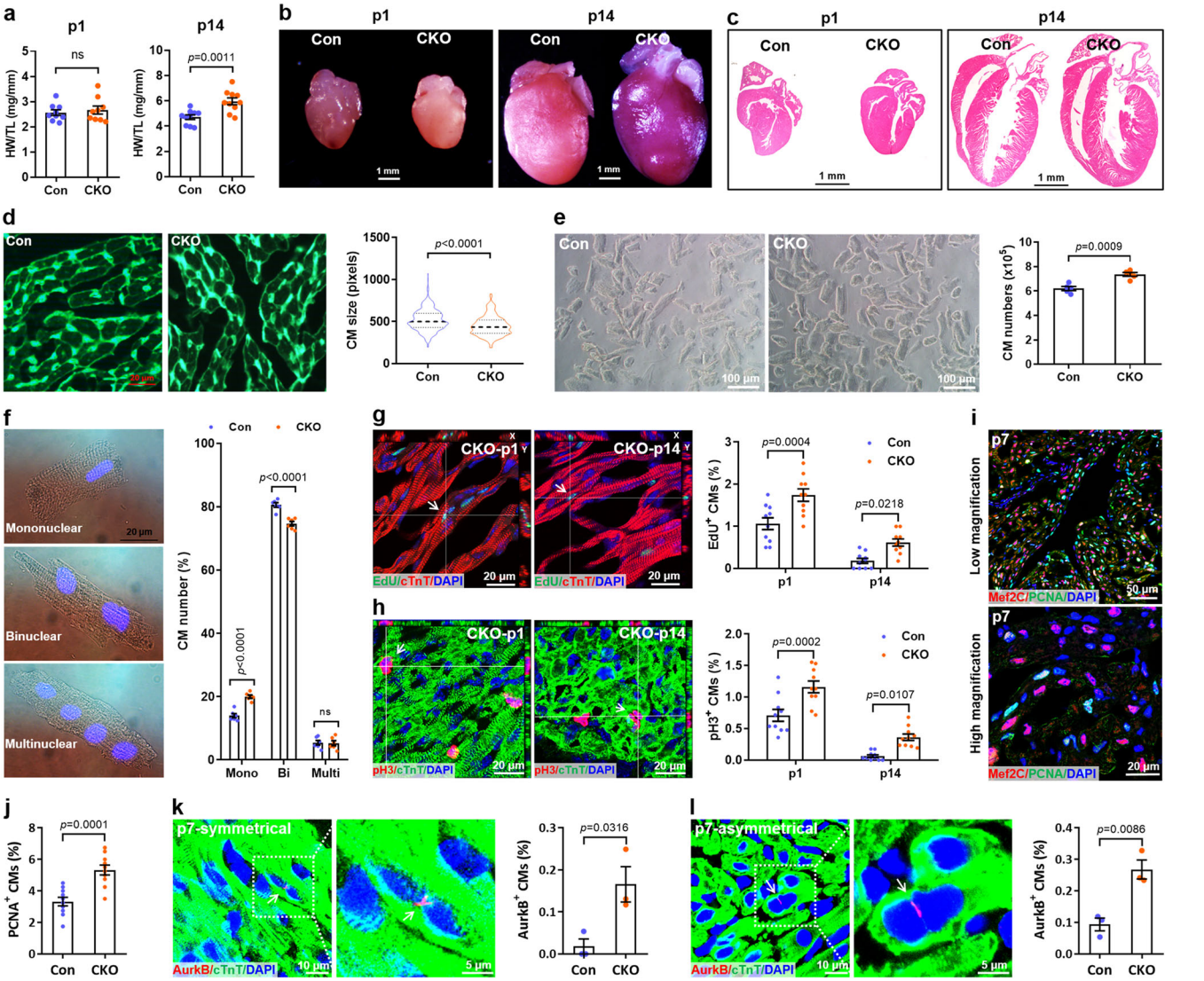

Fig. 2 | Effects of FoxO3 knockout on heart growth in postanal mice. a Heart weight to tibial length (HW/TL) ratio in control and CKO mice at p1 and p14, respectively ($n = 9$ mice for p1 and 10 mice for p14). **b** Representative whole images of control and CKO postnatal hearts at p1 and p14. **c** Representative H&E staining images of control and CKO postnatal hearts at p1 and p14. **d** Representative WGA staining images (upper panel) and quantification (lower panel) of cardiomyocyte size in ventricles at p14 (total ~500 cells in 6 hearts per group). **e** Representative images of cardiomyocytes completely dissociated from whole heart (left panel) and quantification of total rod-shaped cardiomyocyte numbers (right panel) in control and CKO mice at p14 ($n = 6$ hearts). **f** Representative images of cardiomyocyte nucleation (left panel) and quantification of mononuclear (Mono), binuclear (Bi), and multinuclear (Multi) cardiomyocytes (right panel) in control and CKO hearts at p14 ($n = 6$ hearts per group). **g, h** Representative confocal images (left) and quantification (right) of EdU^+ (**g**) and $pH3^+$ (**h**) cardiomyocytes in control and CKO apical ventricles at p1 and p14 ($n = 10$ hearts). **i** Representative confocal images at low (left) and high (right) magnification of $PCNA^+$ cardiomyocytes in CKO apical ventricles. **j** Quantification of $PCNA^+$ cardiomyocytes in control and CKO apical ventricles at p7 ($n = 10$ hearts). **k, l** Representative confocal images (left) and quantification (right) of symmetrical (**k**) and asymmetrical (**l**) $AurkB^+$ cardiomyocytes in control and CKO apical ventricles at p7 ($n = 3$ hearts). All data are presented as the mean ± SEM. *P* values are from two-tailed *t* test (**a**, **d**, **e**, **j**–**l**) or two-way ANOVA followed by Sidak's multiple comparisons test (**f**–**h**). ns, no significant difference. Source data are provided as a Source data file.

antigen (PCNA) and myocyte enhancer factor 2 C (Mef2C) double staining (Fig. 2i, j). To further determine whether FoxO3 knockout can promote the cytokinesis of cardiomyocytes at p7, Aurora Kinase B (AurkB) staining were performed. AurkB analysis can distinguish cardiomyocytes that were undergoing karyokinesis with subsequent cytokinesis (symmetric AurkB) from ones without cytokinesis (asymmetric AurkB)[31]. Our data showed that FoxO3 knockout significantly elevated the percentage of symmetric AurkB-positive cardiomyocytes, implying the increased cytokinesis of cardiomyocytes in CKO heart at p7 (Fig. 2k). Moreover, increased multinucleation (asymmetric AurkB) events were also observed in CKO heart (Fig. 2l). Taken together, these in vivo findings demonstrated that FoxO3 might negatively regulate cardiomyocyte proliferation in early postnatal mice.

FoxO3 knockout improve cardiac function in homeostatic adult mice

Above observation in early postnatal mice prompts us to explore whether FoxO3 knockout influences cardiac function in homeostatic adult mice. For 6-week-old adult mice, we found that heart weight indices (HW/TL) and overall heart size increased in CKO mice compared with controls (Fig. 3a, b). However, there were not significant differences in the expression of myocardial hypertrophy markers including ANP, BNP, and Myh7 between CKO and Con mice (Fig. 3c). WGA staining (Fig. 3d) and cardiomyocyte morphology (Fig. 3e) revealed that cardiomyocyte size was smaller in CKO hearts than that in controls. These data imply that FoxO3 deficiency-increased proliferation of cardiomyocytes in early postnatal mice might lead to

https://doi.org/10.1038/s41467-025-57962-9

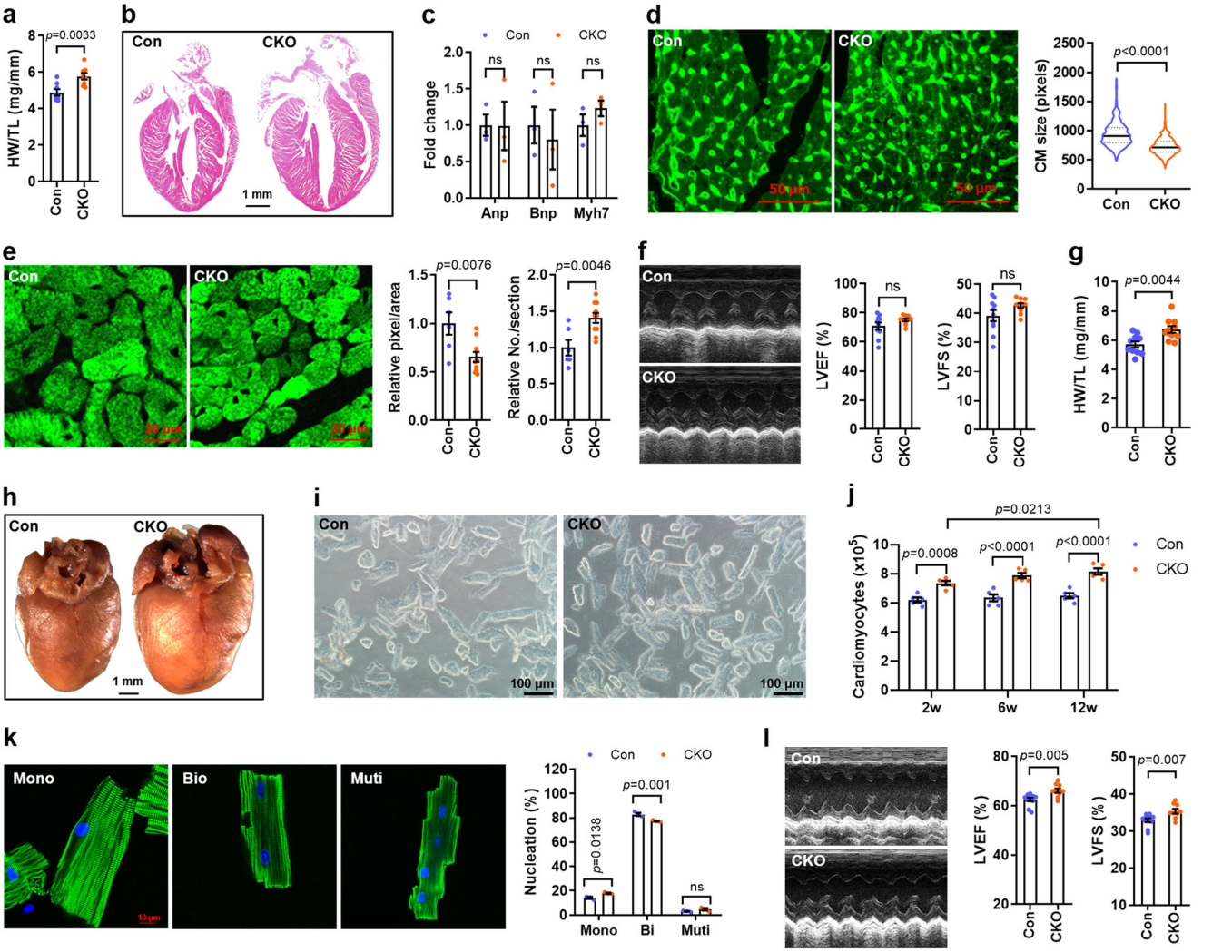

Fig. 3 | FoxO3 knockout promotes cardiac function in adult mice. a HW/TL ratio in control and CKO mice at postnatal week 6 ($n = 8$ mice). **b** Representative images of H&E staining of sections from control and CKO hearts at postnatal week 6. **c** The qPCR validation of hypertrophic markers including *Anp*, *Bnp*, and *Myh7* in control and CKO ventricles at postnatal week 6 ($n = 3$ hearts). **d** Representative WGA staining images (left) and quantification (right) of the size of cardiomyocytes located in ventricles at postnatal week 6 (total ~700 cells in 6 hearts per group). **e** Representative cross section of cTnT staining cardiomyocytes (left) and the quantification of cardiomyocyte size and density (right) in ventricles at postnatal week 6 ($n = 6$ hearts for control and 10 hearts for CKO). **f** Representative images of M-model echocardiography (left) and quantification (right) of LVEF and LVFS levels at postnatal week 6 ($n = 10$ hearts). **g** HW/TL ratio in control and CKO mice at postnatal week 12 ($n = 10$ mice). **h** Representative whole images of adult hearts at postnatal week 12. **i** Representative images of cardiomyocytes completely dissociated from whole heart in control and CKO mice at postnatal week 12. **j** Quantification of total cardiomyocytes in control and CKO mice from 2 to 12 weeks ($n = 5$ hearts). **k** Representative images of cardiomyocyte nucleation (left) and quantification of mononuclear (Mono), binuclear (Bi), and multinuclear (Multi) cardiomyocytes (right) in control and CKO hearts at postnatal week 12 ($n = 3$ hearts). **l** Representative images of M-model echocardiography (left) and quantification of LVEF and LVFS levels (right) at postnatal week 12 ($n = 10$ hearts). All data are presented as the mean ± SEM. *P* values are from two-tailed *t* test (**a**, **d**–**g**, **l**) or two-way ANOVA followed by Sidak's multiple comparisons test (**c**, **j**, **k**). ns, no significant difference. Source data are provided as a Source data file.

increases in cardiomyocyte number and heart size at adult stage. However, cardiac functions were unaffected by FoxO3 knockout in 6-week-old mice (Fig. 3f), indicating that FoxO3 knockout-induced cardiomyocyte proliferation in neonatal mice might need longer time to affect cardiac function at adult stage. We therefore further analyzed the cardiac functions in 12-week-old mice. Histological and morphological analysis revealed that the overall heart size and heart weight indices (HW/TL) were increased in CKO mice compared with controls (Fig. 3g, h). To determine whether FoxO3 knockout increases the total number of cardiomyocytes, cardiomyocytes were isolated from CKO and Con mice (12-week-old) using collagenase digestion. Cell counting revealed a significant increase in the total number of cardiomyocytes in 12-week-old CKO hearts compared with controls (Fig. 3i, j). Moreover, significant increased cardiomyocytes numbers were detected in 12-week-old CKO mice compared with 2-week-old CKO mice, although there were no significant differences between 6- and 2-week-old CKO mice (Fig. 3j). In contrast with CKO mice, no significant differences in cardiomyocyte numbers were detected in adult (6- and 12-week-old) control mice when compared with 2-week-old mice (Fig. 3j). These data imply that the cardiomyocyte number continues to increase from 2- to 12-week-old CKO mice in a lower speed. This was accompanied by the increased percentage of mononucleated cardiomyocytes and the decreased percentage of binucleated cardiomyocytes in CKO hearts (Fig. 3k). Importantly, increased cardiac function was also detected in CKO mice compared with controls (Fig. 3l). Collectively, these results demonstrated that FoxO3 knockout promotes the proliferation of cardiomyocytes at neonatal stage, thereby leading to an increased cardiomyocyte number and cardiac function at adult stage.

https://doi.org/10.1038/s41467-025-57962-9

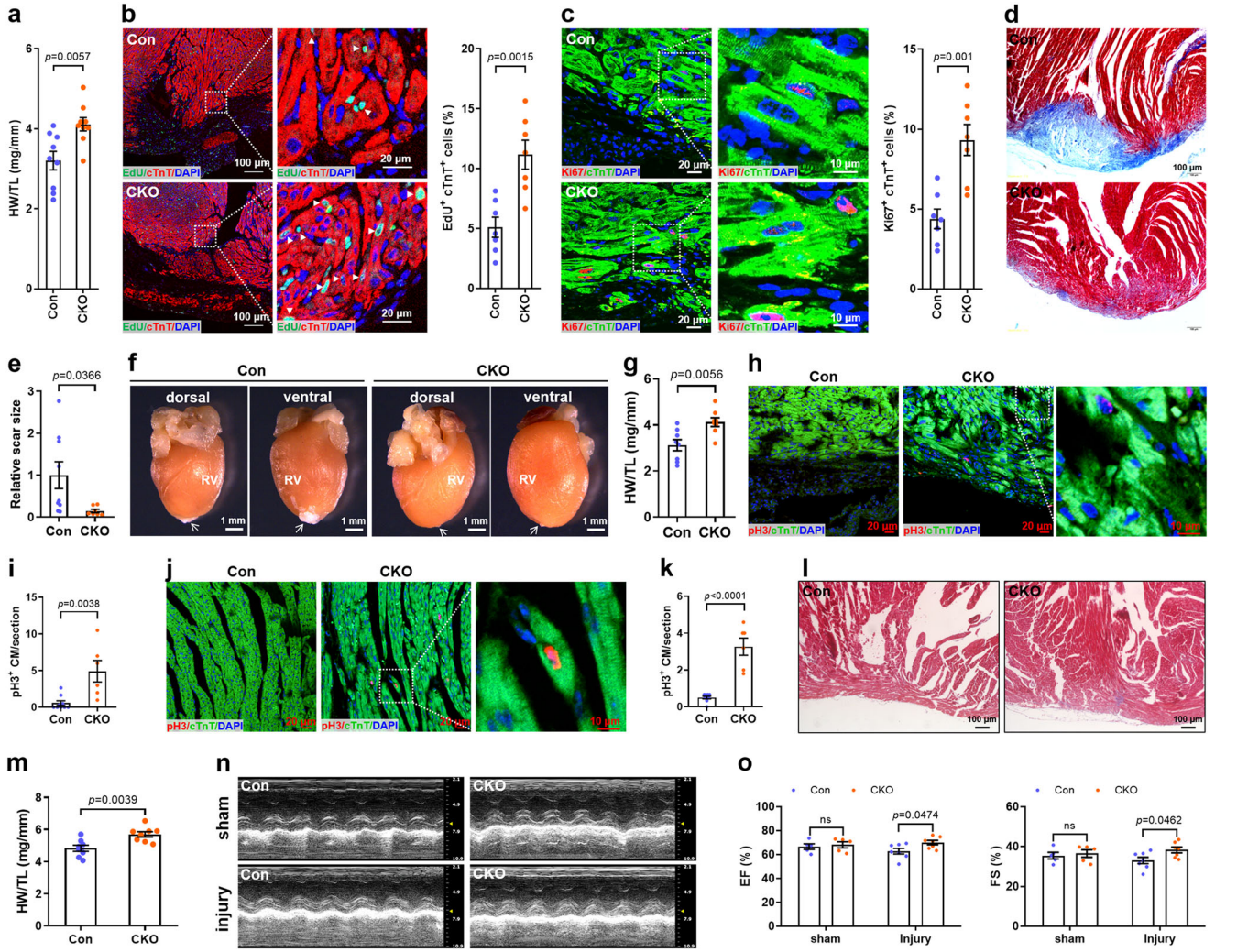

Fig. 4 | FoxO3 knockout promotes heart regeneration in postnatal mice following apical resection at p1. a HW/TL ratio in control and CKO mice at 5 dpr ($n = 9$ mice). **b** Representative images (left) and quantification (right) of EdU$^+$ cardiomyocytes in control and CKO apical ventricle at 5 dpr ($n = 7$ hearts). **c** Representative images (left) and quantification (right) of Ki67$^+$ cardiomyocytes in control and CKO apical ventricle at 5 dpr ($n = 7$ hearts). **d**, **e** Representative Mason's trichrome staining images of cardiac apex (**d**) and quantification of scar size (**e**) in control and CKO hearts at 14 dpr ($n = 9$ hearts for control and 7 hearts for CKO). **f**, **g** Representative whole images of postnatal hearts (**f**, arrows denote scar) and quantification of HW/TL ratio (**g**) at 14 dpr ($n = 7$ mice). **h**–**k** Representative images (**h**, **j**) and quantification (**i**, **k**) of pH3$^+$ cardiomyocytes in the apical (**h**, **i**) and remote (**j**, **k**) zone of control and CKO ventricles at 14 dpr ($n = 9$ hearts for control and 6 hearts for CKO). **l**, **m** Representative Masson's trichrome staining images of cardiac apex (**l**) and quantification of HW/TL ratio (**m**) in control and CKO hearts at 28 dpr ($n = 8$ mice). **n**, **o** Representative images of M-model echocardiography (**n**) and quantification (**o**) of LVEF and LVFS levels in control and CKO mice at 28 dpr ($n = 5$ mice for sham and 7 mice for CKO). All data are presented as the mean ± SEM. *P* values are from two-tailed *t* test (**a**–**c**, **e**, **g**, **i**, **k**, **m**) or two-way ANOVA followed by Sidak's multiple comparisons test (**o**). ns, no significant difference. Source data are provided as a Source data file.

FoxO3 knockout accelerates heart regeneration at regenerative stage

Increased cardiomyocyte proliferation in CKO neonatal mice prompts us to ask whether FoxO3 knockout improves heart regeneration. Firstly, ventricular apex was resected at p1, followed by histological analysis, cardiomyocyte proliferation, and cardiac function evaluation at 5 dpr, 14 dpr, and 28 dpr, respectively. We found that FoxO3 knockout significantly increased the HW/TL ratio at 5 dpr (Fig. 4a). However, the expression of myocardial hypertrophy markers and proinflammatory factors was not significantly changed in CKO hearts compared with controls (Supplementary Fig. 5a, b). EdU incorporation assay revealed that FoxO3 knockout increased the percentage of EdU-positive cardiomyocytes in apical areas at 5 dpr (Fig. 4b). This was consistent with an increase in the percentage of Ki67-positive cardiomyocytes in apical areas in CKO heart compared with controls (Fig. 4c). Consistent with these results at 5 dpr, histological and morphological analysis revealed that scar size was significantly decreased in CKO hearts at 14 dpr compared with control hearts (Fig. 4d–f). Moreover, increased HW/TL ratio was also detected in CKO mice at 14 dpr (Fig. 4g). We also analyzed cardiomyocyte proliferation by pH3 staining and found that FoxO3 knockout increased the numbers of pH3-positive cardiomyocytes in cardiac apical and remote areas (Fig. 4h–k), which indicates that FoxO3 knockout promotes cardiomyocyte proliferation at 14 dpr. However, no significant difference in coronary density was detected in CKO heart at 14 dpr compared with controls (Supplementary Fig. 5c, d). We further extended the repairing period to 28 dpr, and found that both Con and CKO mice greatly regenerated the injured heart without fibrosis (Fig. 4l). Moreover, the increased HW/TL ratio was detected in CKO mice (Fig. 4m), which may imply the improved cardiac function. As expected, left ventricular systolic function was significantly increased in CKO mice, as evaluated by significant increases in left ventricular ejection fraction (LVEF) and

fractional shortening (LVFS) levels, although there were no significant differences in cardiac function between the sham-operated CKO and control mice (Fig. 4n, o). Taken together, these findings indicate that the increased cardiomyocyte proliferation and decreased scar size caused by FoxO3 knockout improves cardiac function, thereby accelerating heart regeneration in neonatal mice.

FoxO3 knockout promotes heart regeneration at non-regenerative stage

To further determine the involvement of FoxO3 in heart regeneration at the non-regenerative stage, ventricular apex resection was performed in postnatal mice at p8, the time point beyond the regenerative windows of neonatal heart. Samples were then collected and analyzed at 5 to 49 dpr (Supplementary Fig. 6a). Significant increase in HW/TL ratio was detected in CKO mice at 5 dpr compared with controls (Supplementary Fig. 6b). EdU incorporation assay revealed that FoxO3 knockout significantly increased the number of EdU-positive cardiomyocytes in both apical and remote areas at 5 dpr (Supplementary Fig. 6c, d), implying increased proliferation of cardiomyocytes in CKO mice. At 21 dpr, the increased HW/TL ratio was detected in CKO mice (Supplementary Fig. 6e). Moreover, increased LVEF and LVFS were detected in CKO mice at 21 dpr compared with controls (Supplementary Fig. 6f), indicating that FoxO3 knockout promotes left ventricular systolic function. Histological analysis revealed that scar size in the cardiac apex at 21 dpr was significantly decreased in FoxO3-deficient hearts compared with controls (Supplementary Fig. 6g), implying the accelerated heart regeneration. Consistent with these results, pH3/cTnT double staining revealed that the percentage of pH3-positive cardiomyocytes was increased in both apical and remote areas in CKO hearts compared with controls (Supplementary Fig. 6h, i). We further extended repairing time to 49 dpr and analyzed cardiac function and regeneration. As expected, apex resection-induced decreases in cardiac function in control mice were significantly restored by FoxO3 knockout, as evidenced by increases in both LVEF and LVFS levels in CKO mice (Supplementary Fig. 6j). In agreement with this result, a significant decrease in scar size was detected in CKO hearts at 49 dpr compared with controls (Supplementary Fig. 6k), indicating a promoted regeneration in CKO heart. In addition, cardiomyocyte sizes were not increased in CKO hearts at 49 dpr compared with controls (Supplementary Fig. 7), indicating that FoxO3 knockout did not lead to cardiac hypertrophy.

To confirm above conclusions in apical resection model, myocardial infarction (MI) model was further performed in p8 mice, followed by sample collection and analysis at the indicated time points (Fig. 5a). Ki67 staining revealed that FoxO3 knockout significantly increased the percentage of Ki67-positive cardiomyocytes in apical areas at 7 days post-MI (dpM), implying the increased cardiomyocyte proliferation in CKO mice (Fig. 5b, d). To prove complete cardiomyocyte proliferation, late cell cycle marker pH3 and cytokinesis marker AurkB were further used in this study. Consistently, the percentage of pH3-positive cardiomyocytes in apical areas was significantly elevated by FoxO3 knockout (Fig. 5c, e), indicating that FoxO3 knockout really promotes the complete proliferation of cardiomyocytes during MI of p8 mice. AurkB staining showed that the percentage of symmetric AurkB-positive cardiomyocytes was significantly increased in cardiac apex in the CKO mice compared with controls, implying the elevated cytokinesis of cardiomyocytes (Fig. 5f). The increased asymmetric AurkB-positive cardiomyocytes was also observed in CKO hearts (Fig. 5g). On the contrary, neither symmetric nor asymmetric AurkB-positive cardiomyocytes were detected in control hearts at 7 dpM (Fig. 5f, g). We also revealed that the expression of proinflammatory factors was not significantly changed in CKO hearts at 7 dpM compared with controls (Supplementary Fig. 8a). Cardiac function analysis showed a modest increase in LVEF and LVFS levels in CKO mice compared with controls at 14 dpM (Fig. 5h). However, significantly increased LVEF and LVFS levels were observed in CKO mice compared with controls at 28 dpM (Fig. 5i), indicating the elevated cardiac function in CKO mice. In agreement with the elevated cardiac function, decreased scar sizes were also detected in CKO hearts at 28 dpM (Fig. 5j), indicating a promoted regeneration in CKO heart. On the contrary, αSMA immunostaining revealed that the angiogenesis capacity was comparable between CKO and control hearts at 28 dpM (Supplementary Fig. 8b). These data from apex resection and MI injury models of p8 mice revealed that FoxO3 knockout can really promote heart regeneration at non-regenerative stage.

To access the pro-regeneration effects of FoxO3 deficiency in adult hearts, $FoxO3^{fl/fl}$ mice were crossbred with inducible Myh6-MerCreMer ($Myh6^{MCM}$) mice to generate $FoxO3^{fl/fl}$::$Myh6^{MCM}$ mice (iCKO), of which the cardiomyocyte-specific knockout of FoxO3 could be induced by tamoxifen administration at the indicated time points. The $Myh6^{MCM}$ mice were used as control (Con). Adult (8-week-old) iCKO and Con mice were injected with tamoxifen (50 mg/kg, i.p.) for 5 days to induce the cardiomyocyte-specific knockout of FoxO3, followed by the permanent ligation of the left anterior descending artery (LAD) to induce myocardium infarction (MI) injury (Fig. 5k). Con mice without MI injury were used as sham group. The inducible knockout of FoxO3 (iCKO) in the injured heart was determined by WB at 7 dpM (Fig. 5l). Ki67 staining showed that FoxO3 knockout greatly increased the proliferation of cardiomyocytes in border zone of infarction at 7 dpM, as indicated by the increased percentage of Ki67-positive cardiomyocytes (Fig. 5m). To confirm this conclusion, cardiomyocyte proliferation was further determined using immunofluorescent staining for pH3, a late cell cycle marker. Almost no pH3-positive cardiomyocytes were detected in control hearts at 7 dpM. However, FoxO3 knockout increased the percentage of pH3-positive cardiomyocytes which indicating the elevated cardiomyocyte proliferation (Fig. 5n). Moreover, MI-induced cardiomyocyte hypertrophy was suppressed by FoxO3 knockout at 7 dpM as indicated by the decreased cardiomyocyte size in iCKO hearts (Fig. 5o). We further analyzed the inflammatory response and revealed that the expression of proinflammatory factors was not significantly changed in iCKO hearts at 7 dpM compared with controls (Supplementary Fig. 9a). To further evaluate the effects of FoxO3 knockout on cardiac function, sham-operated and injured mice were subjected to echocardiography analysis from 0 to 28 dpM. Our data showed that FoxO3 knockout leads to significant increases in LVEF and LVFS levels at 14 and 28 dpM when compared with control hearts (Fig. 5p, q). In line with these results, decreased scar size was also detected in iCKO hearts at 28 dpM when compared with control hearts (Fig. 5r and Supplementary Fig. 10). In contract, the angiogenesis capacity in iCKO heart was comparable with that in control hearts at 28 dpM (Supplementary Fig. 9b). These findings further validate the pro-regeneration effect of FoxO3 inactivation in adult heart.

Variations in FoxO3-regulated genes in postnatal hearts

To investigate target genes involved in FoxO3-mediated heart regeneration in postnatal mice, ventricles isolated from Con and CKO mice at p1 and p14 were subjected to RNA-seq analysis. We identified 646 upregulated and 1871 downregulated genes in Con mice at p14 compared with p1 (Supplementary Fig. 11a). Gene ontology (GO) and KEGG pathway enrichment analysis revealed that heart growth-induced differentially expressed (DE) genes in Con postnatal mice were significantly enriched for cell cycle-related gene sets where 80 genes were specifically identified in postnatal heart at p14 (Supplementary Fig. 11b, c). At p1, 989 upregulated and 1259 downregulated genes were identified in CKO hearts compared with controls (Supplementary Fig. 11d). GO and KEGG analysis revealed that FoxO3 knockout-induced DE genes in neonatal hearts at p1 were significantly enriched for cell growth- and cell cycle-related gene sets where 59 genes were specifically identified in CKO hearts at p1 (Supplementary Fig. 11e, f). At p14, 685 upregulated and 1228 downregulated genes were identified in

https://doi.org/10.1038/s41467-025-57962-9

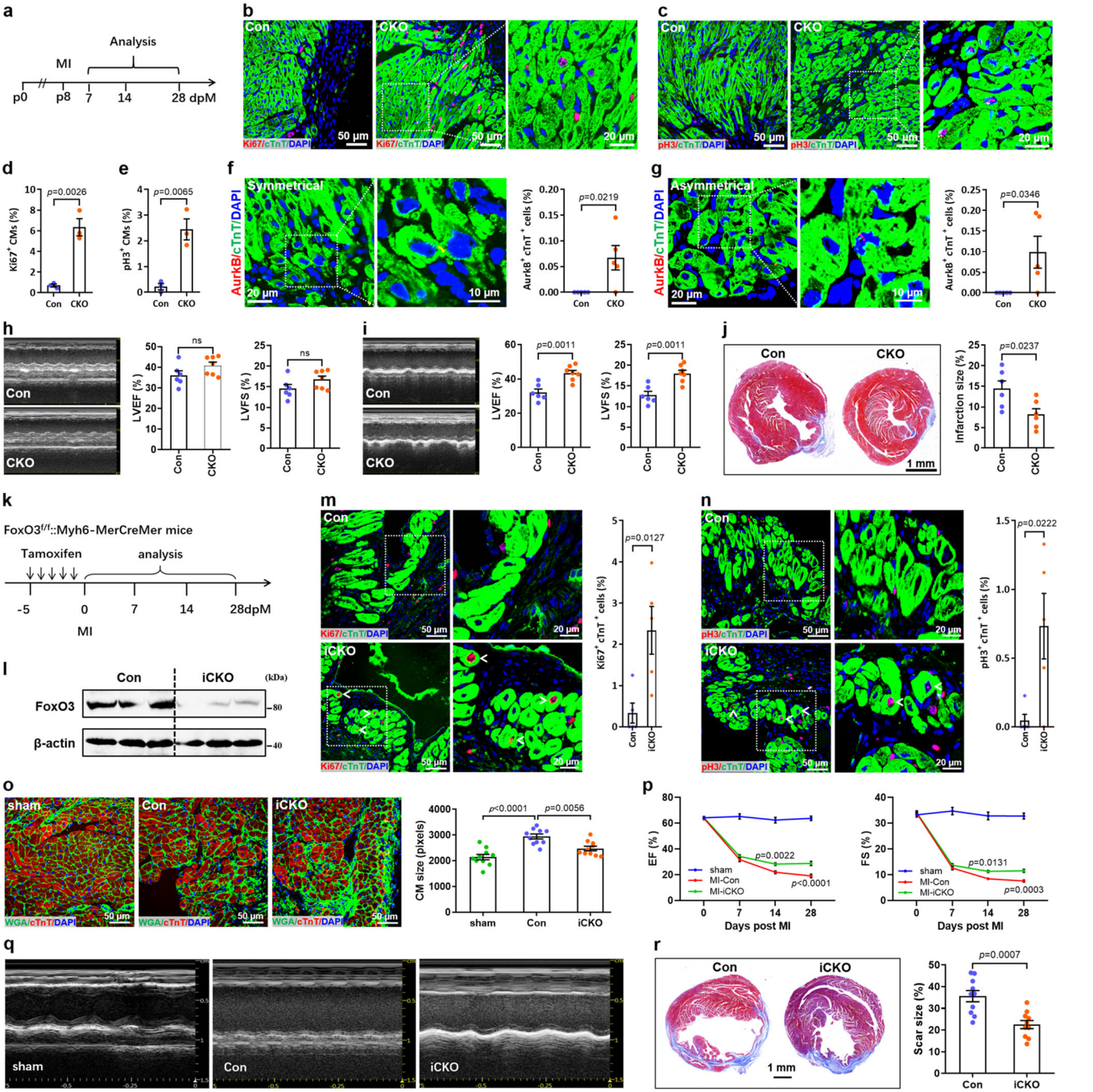

Fig. 5 | FoxO3 knockout improves heart regeneration following MI injury at non-regenerative stage. a Schematic of sample collection and analysis at indicated time points after MI surgery at p8. **b**, **d** Representative images (**b**) and quantification (**d**) of Ki67$^+$ cardiomyocytes in the border zone of infarcted hearts at 7 dpM ($n = 3$ hearts). **c**, **e** Representative images (**c**) and quantification (**e**) of pH3$^+$ cardiomyocytes in the border zone of infarcted hearts at 7 dpM ($n = 3$ hearts). **f**, **g** Representative images (left) and quantification (right) of symmetrical (**f**) and asymmetrical (**g**) AurkB$^+$ cardiomyocytes in the border zone of infarcted hearts at 7 dpM ($n = 5$ hearts). **h**, **i** Representative images of M-model echocardiography (left) and quantification (right) of LVEF and LVFS levels in control and CKO mice at 14 (h) and 28 (i) dpM ($n = 6$ mice for Con and 7 mice for CKO). **j** Representative Masson's trichrome staining images (left) and quantification of scar size (right) at 28 dpM ($n = 6$ mice). **k** Schematic of sample collection and analysis at indicated time points after MI surgery in adult iCKO mice. **l** Validation of the inducible knockout of FoxO3 in heart tissues. **m**, **n** Representative images (left) and quantification (right) of Ki67$^+$ (**m**) and pH3$^+$ (**n**) cardiomyocytes in the border zone of infarcted hearts in iCKO mice at 7 dpM ($n = 5$ hearts). **o** Representative WGA staining images (left) and quantification (right) of cardiomyocyte size in the border zone of infarcted hearts at 7 dpM ($n = 10$ mice). **p** Quantification of LVEF and LVFS levels in control and iCKO mice from 0 to 28 dpM ($n = 10$ mice). Control mice without MI injury were used as sham group ($n = 6$ mice). **q** Representative images of M-model echocardiography in control and iCKO mice at 28 (P) dpM. **r** Representative Masson's trichrome staining images (left) and quantification of scar size (right) in control and iCKO mice at 28 dpM ($n = 10$ mice). All data are presented as the mean ± SEM. *P* values are from two-tailed *t* test (**d**–**j**, **m**, **n**, **r**), one-way ANOVA followed by Tukey's multiple comparisons test (**o**), or two-way ANOVA followed by Sidak's multiple comparisons test (**p**). Source data are provided as a Source Data file.

CKO hearts compared with controls (Supplementary Fig. 11g). In agreement with GO and KEGG data from p1, FoxO3 knockout-induced DE genes were significantly enriched for cell cycle-related gene sets where 36 genes were specifically identified in CKO hearts at p14 (Supplementary Fig. 11h, i). These data suggest that cell cycle-associated genes may play important roles in the regulation of heart regeneration in a FoxO3-dependent manner. As expected, gene-set enrichment analysis (GSEA) further revealed that cell cycle and proliferation gene sets are associated with FoxO3-mediated postnatal heart growth which spanning the regenerative window (Supplementary Fig. 12). Using qPCR assay, we further confirmed the downregulation of several cyclin-dependent kinase inhibitors (CDKN) including Cdkn2 and Cdkn3 in CKO hearts at p1 and/or p14 compared with controls (Supplementary Fig. 11j, k). To further determine this idea in adult heart, the expression of cell cycle-related genes was examined in 2-month-old CKO mice. The qPCR analysis revealed that the expression of negative regulators of cell cycle including Cdkn2a, Cdkn2b, and Cdkn3 in adult heart were significantly reduced by FoxO3 knockout compared with controls, implying the increased proliferation levels in CKO hearts (Supplementary Fig. 13). These findings indicate that specific knockout of FoxO3 in cardiomyocytes can reduce the expression of negative regulators of cell cycle in postnatal hearts. However, FoxO3 knockout did not influence the expression of Meis1 in postnatal heart (Supplementary Fig. 11j, k), which has been demonstrated to be important for the regulation of postnatal cardiomyocyte cell cycle arrest[15].

It has been demonstrated that sarcomere genes (TNNI3, MYL2, TNNT2, MYOZ2, TPM1, and ACTC1) and fatty acid oxidation (FAO) genes (CPT1A, CPT1B, and SLC27A) are crucial for cardiomyocyte maturation and contraction[32,33]. We thus analyzed the expression of these genes using primary cardiomyocytes isolated from control and CKO mice. We found that two sarcomere genes (TNNT2 and MYOZ2) and two FAO genes (CPT1A and SLC27A) were upregulated in FoxO3-deficient cardiomyocytes within postnatal day 14, whereas there were no significant differences in the expression levels of these genes between adult wild-type and mutant cardiomyocytes (Supplementary Fig. 14). These findings imply that certain sarcomere and FAO genes might be influenced by FoxO3 in postnatal rather than in adult hearts.

Previous study has reported the antagonistic functions between FoxO1 and FoxM1 in neonatal cardiomyocyte cell cycle withdrawal, and demonstrated the requirement of FoxM1 for cardiomyocyte proliferation[34]. Moreover, it has been demonstrated that FoxM1 is required for heart regeneration through transcriptional regulation of pro-proliferative genes including G2-phase genes (Ccnf and G2e3) and M-phase genes (Cenpf and Prc1)[35]. These previous findings imply the potential mutual antagonism between FoxO3 and FoxM1. This prompts us to ask whether FoxO3-deficiency-mediated cardiomyocyte proliferation is contributed by the potential upregulation of FoxM1 under our experimental conditions. To determine the expression of FoxM1 in cardiomyocytes with or without FoxO3 knockout, primary cardiomyocytes isolated from control and CKO neonatal mice at p1 were subjected to qPCR assay. We found that FoxO3 deficiency has no significant effects on the expression of FoxM1 in neonatal cardiomyocytes. Consistently, the expression levels of FoxM1-dependent cell cycle genes are comparable between control and FoxO3-deficient neonatal cardiomyocytes (Supplementary Fig. 15a). To further determine the expression of FoxM1 and its downstream targets in cardiomyocytes upon heart injury, we performed apical resection in p1 neonatal mice and isolated primary cardiomyocytes at 5 dpr. Our data showed that both FoxM1 and its targets expression in cardiomyocytes were comparable between control and CKO groups (Supplementary Fig. 15b). Taken together, these results suggest that the increased proliferation of cardiomyocytes and promoted cardiac regeneration in FoxO3-deficient mice may be independent of FoxM1 signaling.

SFRP2 contributes to FoxO3-mediated cardiomyocyte proliferation

To further identify potential target genes involved in FoxO3-mediated heart regeneration in postnatal mice, downregulated genes in CKO ventricles at p1 (1259 genes) and p14 (1228 genes) versus controls were subjected to GO analysis, respectively. Given that FoxO3 deficiency promotes cardiomyocyte proliferation in vitro (Supplementary Fig. 2) and in vivo (Figs. 2 and 4), we speculate that negative regulators of cardiomyocyte proliferation might be downregulated by FoxO3 deficiency. Therefore, we subsequently focused on the gene sets associated with negative regulation of cell proliferation (NRP) and growth (NRG) in GO terms from the downregulated genes in CKO ventricles at p1 and p14 (Supplementary Tables 1 and 2). NRP- and NRG-related genes from CKO versus Con ventricles at p1 and p14 were compared. Four potential target genes including Trp53, Sfrp2, Cdkn2c, and Cdkn2d were screened by Venn Diagram between different gene sets (Fig. 6a). To elucidate whether and how FoxO3 regulates the expression of these potential targets, we analyzed their promoter sequence and identified a series of FoxO3 binding sites (Supplementary Tables 3–6). The binding site with the highest score for each target was then analyzed by ChIP-qPCR to examine the in vivo interaction between FoxO3 and target gene promoters. Primary cardiomyocytes were isolated from sham and injured control mice at 5 dpr for ChIP-qPCR assay. Among these four potential targets, our data revealed the interaction between FoxO3 proteins and the promoters of Trp53, Sfrp2, and Cdkn2c instead of Cdkn2d in primary cardiomyocytes isolated from sham-operated hearts, as verified by increases in the relative signals of FoxO3 compared to IgG (Fig. 6b). Moreover, only Trp53 and Sfrp2 showed decreases in the interaction with FoxO3 protein in primary cardiomyocytes isolated from injured heart at 5 dpr compared with cardiomyocytes from sham group (Fig. 6b), suggesting that FoxO3-mediated expression of Trp53 and Sfrp2 in cardiomyocytes may be regulated by the stress of cardiac injury. Among these four genes, the most enrichment of FoxO3 signal relative to IgG signal in sham group was detected for Sfrp2 promoter (Fig. 6c). In addition, we found a moderate decrease in Trp53 expression and a remarkable decrease in Sfrp2 expression in primary cardiomyocytes isolated from CKO mice compared with controls (Fig. 6d). These data suggest that Trp53 and Sfrp2 may be the downstream targets of FoxO3 in regulating cardiomyocyte proliferation. As expected, GSEA analysis revealed that Trp53 and Sfrp2 pathways were significantly associated with FoxO3-mediated postnatal heart growth which spanning the regenerative window (Fig. 6e, f). To further address the effects of FoxO3 on target gene expression, we constructed luciferase reporter plasmids using target gene promoters which include FoxO3 binding sites. Reporter gene assay revealed that FoxO3 overexpression greatly promoted relative luciferase activity driven by the promoter of Trp53 and Sfrp2 (Fig. 6g). Mutation of the consensus FoxO3 binding site with highest score in the promoter of Sfrp2 attenuated the FoxO3 overexpression-induced increase in luciferase activity (Fig. 6g). However, the mutation of FoxO3 binding site with highest score in Trp53 promoter (Trp53△1) failed to attenuate the luciferase activity induced by FoxO3 (Fig. 6g). To further determine the effects of other potential binding sites in Trp53 promoter, we further mutated the other binding site with the second higher score and constructed the new reporter plasmid (pTrp53△2-GR) for further reporter gene assay. We found that FoxO3 overexpression-induced increase in luciferase activity could be reduced by the second mutation (Trp53△2) (Fig. 6g). These findings suggest that the second FoxO3 binding site in Trp53 promoter may be more critical for Trp53 regulation. In agreement with mouse, FoxO3 binding sites in Trp53 and Sfrp2 promoters could also be predicted in other organisms including human, frog, and zebrafish, implying the evolutionary conservation of Foxo3 binding with the promoters of these two targets (Supplementary Fig. 16, Supplementary Tables 7 and 8).

Given that the most enrichment of FoxO3 signal in Sfrp2 promoter (Fig. 6c) and the highest inhibition of Sfrp2 expression in

https://doi.org/10.1038/s41467-025-57962-9

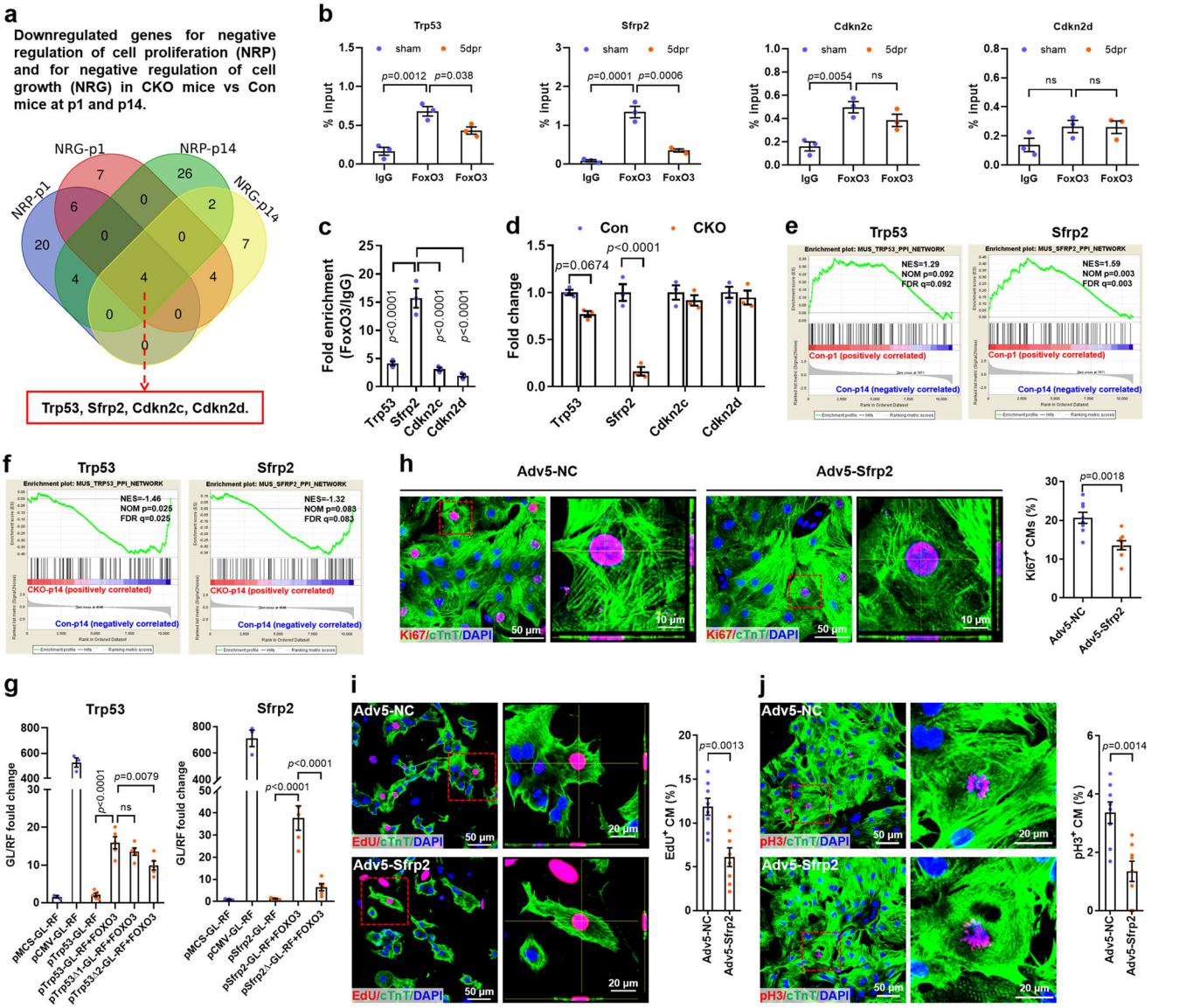

Fig. 6 | Targets screening for FoxO3-mediated cardiac regeneration in postnatal mice. a RNA-seq identified 4 overlapping genes (Trp53, Sfrp2, Cdkn2c, and Cdkn2d) between the downregulated gene sets for *n*egative *r*egulation of cell *p*roliferation (NRP) and *g*rowth (NRG) in CKO ventricles versus controls at p1 and p14. **b** ChIP-qPCR validation of FoxO3 binding to the promoters of the identified 4 potential targets in primary cardiomyocytes isolated from sham and injured hearts at 5 dpr ($n = 3$). **c** Fold enrichment of FoxO3 signal relative to IgG signal for these 4 potential target promoters in cardiomyocytes isolated from sham-operated hearts ($n = 3$). **d** The qPCR validation of these 4 potential targets expression in control and CKO cardiomyocytes at 5 dpr ($n = 3$). **e**, **f** GSEA analysis based on the RNA-seq data revealed that Trp53 and Sfrp2 pathways are associated with FoxO3-mediated postnatal heart regeneration. **g** The interactions of FoxO3 with the promoters of Trp53 and Sfrp2 are evaluated using reporter gene and mutation assay ($n = 5$). **h**–**j** Primary cardiomyocytes isolated from CKO neonatal mice at p1 are transfected with Adv5-NC and Adv5-Sfrp2 adenoviruses for 48 h, followed by immunofluorescent staining for cTnT to verify cardiomyocytes, for proliferation markers Ki67 (**h**), EdU (**i**), and pH3 (**j**) to verify proliferating activity of cardiomyocytes. Representative images (left) and quantification (right) of proliferating cardiomyocytes in Adv5-NC and Adv5-Sfrp2 groups are shown ($n = 8$). All data are presented as the mean ± SEM. *P* values are from two-tailed *t* test (**h**–**j**), one-way ANOVA followed by Tukey's multiple comparisons test (**b**, **c**, **g**) or two-way ANOVA followed by Sidak's multiple comparisons test (**d**). ns, no significant difference. Source data are provided as a Source Data file.

FoxO3-deficient cardiomyocytes (Fig. 6d), Sfrp2 was further analyzed in the following experiments. To determine the effect of Sfrp2 on cardiomyocyte proliferation, primary cardiomyocytes isolated from wild-type neonatal mice at p1 were treated with siRNA targeting Sfrp2 (siSfrp2). We found that Sfrp2 knockdown (Supplementary Fig. 17a) significantly promoted cardiomyocyte proliferation as evidenced by the increased percentage of Ki67-positive cardiomyocytes (Supplementary Fig. 17b, c). In agreement with this result, downregulation of Sfrp2 expression (Supplementary Fig. 18) and increase in cardiomyocytes proliferation (Fig. 2) was detected in CKO ventricles when compared with controls. Thus, we supposed that Sfrp2 might be responsible for FoxO3-medicated cardiomyocyte proliferation. To further elucidate whether and how Sfrp2 influences the proliferation of FoxO3-deficient cardiomyocytes, we overexpressed Sfrp2 using adenovirus type 5 (Adv5) in the primary cardiomyocytes isolated from CKO neonatal mice at p1 (Supplementary Fig. 19). Ki67/cTnT double staining revealed that the percentage of Ki67-positive cardiomyocytes was decreased by Sfrp2 overexpression (Fig. 6h), implying the decreased proliferation of Sfrp2-overexpressing cardiomyocytes. Consistent with the result, EdU incorporation assay showed that the percentage of EdU-positive cardiomyocytes was significantly decreased in Adv5-Sfrp2 group compared with Adv5-NC group

https://doi.org/10.1038/s41467-025-57962-9

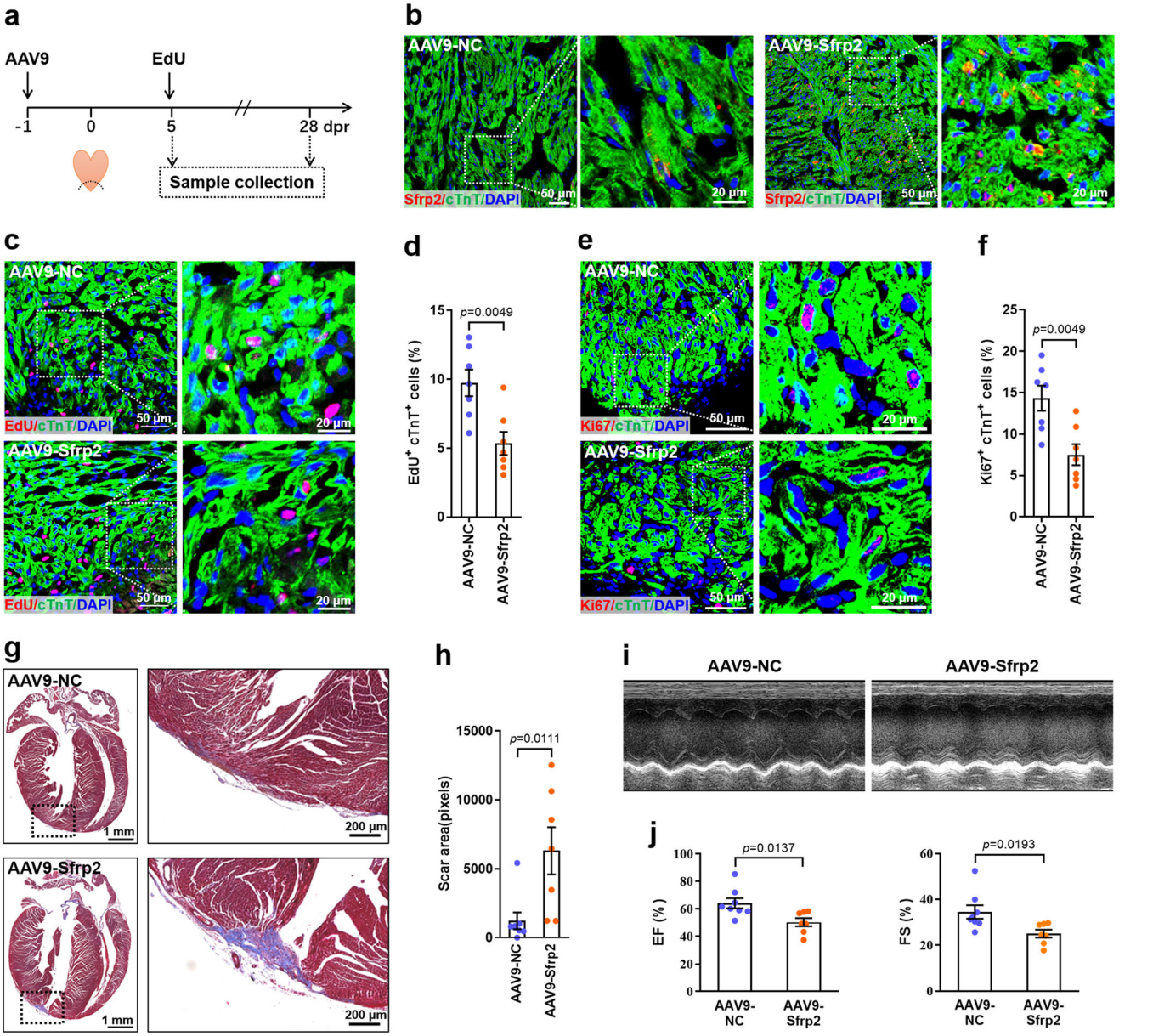

Fig. 7 | Sfrp2 overexpression suppresses cardiac regeneration in FoxO3-deficient postnatal mice. a Schematic of AAV9 virus injection in CKO postnatal mice at p1, apex resection at p2 (equal to 0 dpr), EdU injection and sample collection at indicated time points. **b** Representative images of Sfrp2 expression mediated by AAV9-NC and AAV9-Sfrp2 viruses in postnatal hearts at 5 dpr. Right panel, magnified confocal images of Sfrp2 expression in left panel. At least three times each experiment was repeated independently with similar results. **c**, **d** Representative images (**c**) and quantification (**d**) of EdU$^+$ cardiomyocytes in the injured apical ventricles at 5 dpr ($n = 7$ hearts). **e**, **f** Representative images (**e**) and quantification (**f**) of Ki67$^+$ cardiomyocytes in the injured apical ventricles at 5 dpr ($n = 7$ hearts). **g**, **h** Representative Masson's trichrome staining images of cardiac apex (**g**) and quantification of scar size (**h**) in AAV9-NC and AAV9-Sfrp2 hearts at 28 dpr ($n = 7$ hearts). **i**, **j** Representative images of M-model echocardiography (**i**) and quantification of LVEF (**j**, left) and LVFS (**j**, right) in AAV9-NC and AAV9-Sfrp2 hearts at 28 dpr ($n = 7$ hearts). All data are presented as the mean ± SEM. *P* values are from two-tailed *t* test (**d**, **f**, **h**, **j**). Source data are provided as a Source data file.

(Fig. 6i). In addition, pH3/cTnT double staining further confirmed that Sfrp2 overexpression inhibited cardiomyocyte proliferation as evidenced by the decreased percentage of pH3-positive cardiomyocytes (Fig. 6j). These findings suggest that FoxO3 deficiency-induced increases in cardiomyocyte proliferation can be significantly restored by Sfrp2 overexpression.

SFRP2 overexpression suppresses heart regeneration in FoxO3-deficient mice

To further determine the effects of Sfrp2 on heart regeneration in FoxO3-deficient mice, we overexpressed Sfrp2 in CKO neonatal mice at p1 using AAV9-Sfrp2 and analyzed the cardiomyocyte proliferation and heart regeneration at 5 and 28 dpr, respectively (Fig. 7a). EdU incorporation assay revealed that in vivo overexpression of Sfrp2 (Fig. 7b) significantly decreased the percentage of EdU-positive cardiomyocytes in ventricular apex at 5 dpr compared with AAV9-NC group (Fig. 7c, d). Moreover, Ki67/cTnT double staining showed that Sfrp2 overexpression suppressed cardiomyocyte proliferation in ventricular apex at 5 dpr, as evidenced by the decreased percentage of Ki67-positive cardiomyocytes in the AAV9-Sfrp2 group (Fig. 7e, f). In line with these results, histological analysis revealed that scar size was significantly increased by Sfrp2 overexpression at 28 dpr compared with AAV9-NC group (Fig. 7g, h). In addition, depraved cardiac function was detected in Sfrp2-overexpressing hearts at 28 dpr as

https://doi.org/10.1038/s41467-025-57962-9

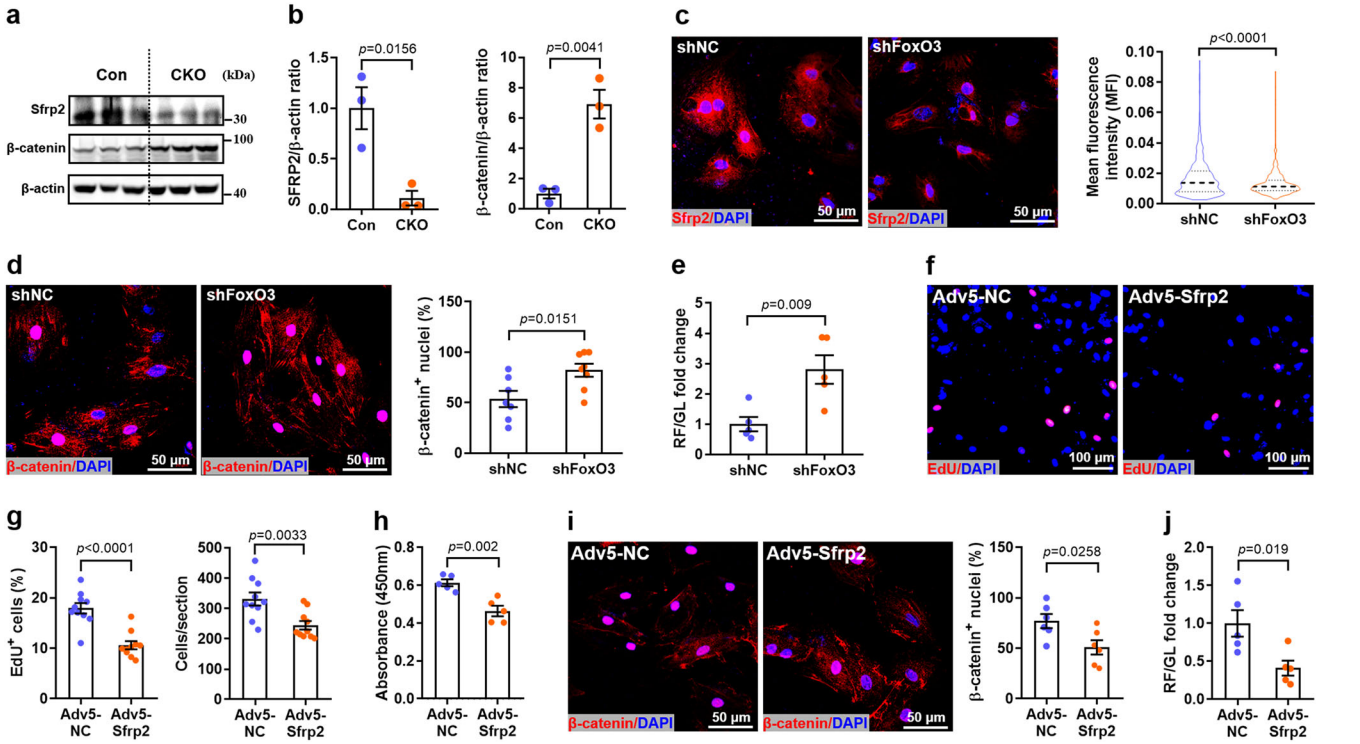

Fig. 8 | FoxO3 knockout enhances the activation of Wnt/β-catenin pathway by suppressing Sfrp2 in cardiomyocytes. a, **b** Representative images (a) and quantification of western blotting for Sfrp2 (**b**, left) and β-catenin (**b**, right) expression in primary cardiomyocytes isolated from neonatal mice at p1 ($n = 3$ mice). **c** Representative images (left) and quantification (right) of immunofluorescent staining for Sfrp2 in control and FoxO3-deficient HL-1 cells ($n = \sim 600$ cells from 8 experiments). **d** Representative images (left) and quantification (right) of immunofluorescent staining for β-catenin in control and FoxO3-deficient HL-1 cells ($n = 8$). **e** The relative activation of β-catenin is evaluated in control and FoxO3-deficient HL-1 cells using TOP-Flash reporter assay ($n = 5$). **f**, **g** Representative images (**f**) and quantification of EdU$^+$ HL-1 cells (**g**, left) and density (**g**, right) in control and Sfrp2-overexpressing cells ($n = 10$). **h** Cell counting assay for control and Sfrp2-overexpressing HL-1 cells ($n = 5$). **i** Representative images (left) and quantification (right) of immunofluorescent staining for β-catenin in control and Sfrp2-overexpressing HL-1 cells ($n = 6$). **j** The relative activation of β-catenin is evaluated in control and Sfrp2-overexpessing HL-1 cells using TOP-Flash reporter assay ($n = 5$). All data are presented as the mean ± SEM. *P* values are from two-tailed *t* test (**b**–**e**, **g**–**j**). Source data are provided as a Source data file.

demonstrated by the decreased LVEF and LVFS values when compared with AAV9-NC groups (Fig. 7i, j). Taken together, these findings suggest that Sfrp2 overexpression suppresses the accelerated heart regeneration in FoxO3-deficient mice.

FoxO3 deficiency promotes Wnt/β-catenin signaling activation by suppressing Sfrp2 in cardiomyocytes

It is well known that secreted frizzled-related protein 2 (Sfrp2) is the inhibitor of canonical Wnt/β-catenin signaling. As expected, GSEA analysis further revealed that Wnt signaling is significantly associated with FoxO3-mediated postnatal heart growth which spanning the regenerative window (Supplementary Fig. 20). This implies that canonical Wnt/β-catenin pathway may be involved in FoxO3/Sfrp2-mediated regulation of heart regeneration in postnatal heart. To determine the effects of FoxO3 on the expression of Sfrp2 and β-catenin, primary cardiomyocytes isolated from control and CKO neonatal mice at p1 was subjected to western blotting assay. Our data showed that FoxO3 knockout greatly reduced the production of Sfrp2. On the contrary, β-catenin production in cardiomyocytes was increased by FoxO3 knockout (Fig. 8a, b). These data imply that FoxO3 might negatively control β-catenin production in cardiomyocytes by promoting Sfrp2 expression. In consistent with primary cardiomyocytes, decreased Sfrp2 and increased β-catenin production were also detected in the FoxO3-deficient HL-1 cell line compared with control cells (Fig. 8c, d). Moreover, the transcriptional activity of endogenous β-catenin was measured by TOP-Flash reporter (Red Firefly luciferase) assays. Increased relative firefly luciferase activity was detected in the FoxO3-deficient HL-1 cells compared with controls (Fig. 8e), which indicating that FoxO3 knockdown significantly promotes β-catenin transcriptional activity.

To further determine whether Sfrp2 influences FoxO3-regulated proliferation of HL-1 cells, we overexpressed Sfrp2 using Adv5 adenovirus in the FoxO3-deficient HL-1 cells. In consistent with primary cardiomyocytes from CKO mice (Fig. 6h–j), we found that Sfrp2 overexpression inhibited the proliferation of FoxO3-deficient HL-1 cells as proved by the decreased percentage of EdU-positive cells and total cell density (Fig. 8f, g). Moreover, cell counting assay also revealed the decreased proliferation in Sfrp2-overexpressing cells compared with controls (Fig. 8h). To determine the influence of Sfrp2 on β-catenin activity, the expression and transcriptional activity of β-catenin were further examined in the FoxO3-deficient HL-1 cells with and without overexpression of Sfrp2. As expected, Sfrp2 overexpression significantly suppressed the expression and nuclear localization of β-catenin as indicated by the decreased percentage of β-catenin-positive nuclei (Fig. 8i). In agreement with this result, TOP-Flash reporter assay further revealed the decreased transcriptional activity of β-catenin in Sfrp2-overexpressing cells (Fig. 8j). These findings suggest that FoxO3 deficiency promotes β-catenin signaling activation by suppressing Sfrp2 in cardiomyocytes, implying the involvement of canonical Wnt/β-catenin pathway.

To further determine whether β-catenin-independent non-canonical Wnt signaling is activated in FoxO3-deficient cardiomyocytes, we examined the activation of JNK (the planar cell polarity (PCP)-dependent non-canonical Wnt pathway) and CaMKII (the Ca^{2+}-dependent non-canonical Wnt pathway)[36] in primary cardiomyocytes isolated from CKO and control neonatal mice. We found that the

phosphorylation of JNK and CaMKII in FoxO3-deficient cardiomyocytes was comparable with that in control cells (Supplementary Fig. 21a, b), implying that non-canonical Wnt signaling may be not involved in the phenotypes mediated by FoxO3-Sfrp2 axis in cardiomyocytes. Previous studies have reported that several Wnt ligands including Wnt1[37], Wnt2b[38], and Wnt10b[39] may be involved in cardiac repair and regeneration. To determine whether these Wnt ligands are involved in the FoxO3-Sfrp2 axis-mediated phenotypes under our experimental conditions, we examined the expression of Wnt1, Wnt2b, and Wnt10b in cardiomyocytes with Sfrp2 silencing. Our data showed that Sfrp2 knockdown has no significant impact on the expression of these three Wnt ligands (Supplementary Fig. 21c, d). To analyze the potential Wnt ligands binding to Sfrp2, we predicted the structure of mouse Sfrp2 and 19 Wnt ligands using AlphaFold3 and calculated the binding affinities between Sfrp2 and Wnt ligands using HDOCK server. Among the 19 Wnt ligands, the prediction data showed that Wnt8a and Wnt4 are the top2 ligands with higher binding affinity for Sfrp2 protein (Supplementary Fig. 21e). We thus examined the expression of these two Wnt ligands in primary cardiomyocytes with Sfrp2 silencing, and found that Sfrp2 silencing significantly increased the production of Wnt8a instead of Wnt4 (Supplementary Fig. 21f, g). These data imply that Sfrp2 may negatively regulate Wnt8a in cardiomyocytes.

Disturbance of endogenous Sfrp2 and β-catenin attenuates cardiomyocyte proliferation in CKO mice

To determine whether downregulation of endogenous Sfrp2 in CKO heart contributes to cardiomyocyte proliferation in vivo, we overexpressed Sfrp2 in CKO mice by injecting AAV9-Sfrp2 viruses at p1 and performed MI surgery at p8, the time point beyond the regenerative windows of neonatal heart. AAV9-NC virus was used as negative control. Cardiomyocyte proliferation in infarct border zone was then analyzed by immunofluorescent staining at 7 dpM (Fig. 9a). Successful overexpression of Sfrp2 in heart tissue at p8 was validated by western blotting validation (Fig. 9b). Ki67 staining showed that Sfrp2 overexpression significantly suppressed cardiomyocyte proliferation, as determined by the decreased percentage of Ki67-positive cardiomyocytes in AAV9-Sfrp2 group compared with AAV9-NC group (Fig. 9c). In consistent with this result, the percentage of pH3-positive cardiomyocytes was significantly decreased by Sfrp2 overexpression (Fig. 9d), indicating that Sfrp2 overexpression really blocks the complete proliferation of cardiomyocytes induced by FoxO3 knockout. These findings suggest that the endogenous downregulation of Sfrp2 indeed contributes to the increased proliferation of cardiomyocytes during heart regeneration of CKO mice at non-regenerative stage.

To confirm the effect of increased endogenous β-catenin on heart regeneration of CKO mice at non-regenerative stage, we inhibited β-catenin expression in CKO mice by injecting AAV9-shRNA targeting β-catenin (AAV9-shβCat) at p1. AAV9-shNC virus was used as negative control. The MI surgery was performed at p8, followed by analysis at 7 and 28 dpM (Fig. 9e). Our data showed that β-catenin knockdown (Fig. 9f) significantly decreased the percentage of Ki67-positive cardiomyocytes at 7 dpM compared with AAV9-shNC group (Fig. 9g). In agreement with Ki67 staining, pH3 staining revealed that β-catenin knockdown greatly suppressed cardiomyocyte proliferation in CKO heart at 7 dpM, as demonstrated by the decreased percentage of pH3-positive cardiomyocytes in AAV9-shβCat group compared with AAV9-shNC group (Fig. 9h). In consistent with these results, Masson's staining showed that β-catenin knockdown increased the scar sizes in CKO hearts at 28 dpM (Fig. 9i and Supplementary Fig. 22), indicating a reduced regeneration in CKO heart. Consistently, significantly decreased LVEF and LVFS levels were observed in β-catenin-deficient CKO mice compared with controls at 28 dpM (Fig. 9j), indicating the deteriorated cardiac dysfunction. These findings suggest that endogenous β-catenin is a mediator of FoxO3 in regulating heart regeneration at non-regenerative stage. To further determine whether β-catenin knockdown counteract the pro-proliferation effect of FoxO3 inactivation in adult hearts, AAV9-shβCat and control viruses were injected into adult CKO mice for 2 weeks, followed by MI surgery and cardiomyocyte proliferation determination at 7 dpM (Supplementary Fig. 23a). Our data showed that β-catenin knockdown (Supplementary Fig. 23b, c) significantly suppressed cardiomyocyte proliferation in adult CKO heart, as determined by the decreased percentage of Ki67- and pH3-positive cardiomyocytes in AAV9-shβCat group compared with that in AAV9-NC group (Supplementary Fig. 23d, e). These findings suggest that the endogenous β-catenin contributes to cardiomyocyte proliferation in FoxO3-deficient adult heart. Taken together, our results indicate that downregulation of Sfrp2 caused by FoxO3 inactivation activates canonical Wnt/β-catenin pathway, which upregulates the expression of genes required for cardiomyocyte proliferation, thereby promoting heart regeneration in mice (Fig. 9k).

Discussion

In the present study, we provided in vitro and in vivo evidence demonstrating the functional importance of FoxO3 in regulating cardiomyocyte proliferation and heart regeneration in postnatal mice upon injury. We found that FoxO3 expression is higher in adult cardiomyocytes than that in neonatal ones. Moreover, FoxO3 activity was reduced in neonatal heart upon injury. FoxO3 deficiency promoted cardiomyocyte proliferation and accelerated heart regeneration in postnatal mice. Our data demonstrated that FoxO3 negatively regulates cardiomyocyte proliferation and heart regeneration by promoting Sfrp2 expression, which leading to the inactivation of canonical Wnt/β-catenin pathway.

FoxO3 is one of Forkhead box O (FoxO) subfamily of transcription factors and is involved in a variety of cellular processes including oxidative stress response, metabolism, apoptosis, and proliferation in different cell types[40]. Previous studies have demonstrated that FoxO3 plays important roles in cardiovascular diseases. Mice globally lacking FoxO3 are viable but develop cardiac hypertrophy at adult stage[23,26], implying that FoxO3 is essential for the integrity and function of heart. However, cardiomyocyte-specific activation of FoxO3 in adult mice resulted in a decrease in heart weight and a reduction in stroke volume and cardiac output through reducing the size of cardiomyocytes[27]. In contrast, activation of FoxO3 protected cardiomyocyte survival under conditions of oxidative stress through induction of antioxidants and cell survival pathways[24]. These data suggest that the function of FoxO3 is complicated in hearts. However, the potential functional importance of FoxO3 and the underlying mechanism during heart regeneration remain largely unclear and need to be further elucidated. FoxO3 is the central mediator of the pro-proliferative PI3K/AKT pathway in which AKT phosphorylation results in inactivation, nuclear exclusion, and subsequent degradation of FoxO3[29]. In this study, we found that FoxO3 predominantly located in the nuclei of cardiomyocytes, but its expression was upregulated in adult heart compared to neonatal heart (Supplementary Fig. 1). Given that the cardiac regeneration capacity in postnatal mice markedly decreases with growth and completely disappears by p7, the expression profile of FoxO3 is contrary to the capacity of cardiac regeneration in postnatal mice. Moreover, FoxO3 phosphorylation and expression were increased by injury in neonatal hearts (Fig. 1), suggesting that FoxO3 activity was decreased during neonatal heart regeneration. FoxO3 deficiency increased the capacity of cardiomyocyte proliferation and heart regeneration in neonatal mice (Figs. 2–4). In addition, increased cardiomyocyte proliferation and improved heart regeneration were also observed in FoxO3-deficient mice that was injured beyond the regenerative windows, implying that FoxO3 deficiency could promote heart regeneration in postnatal mice at a non-regenerative stage (Fig. 5 and Supplementary Fig. 6). These findings indicate that FoxO3 might negatively control cardiomyocyte proliferation and heart regeneration in postnatal mice. This idea is consistent with the previous reports showing that FoxO3

https://doi.org/10.1038/s41467-025-57962-9

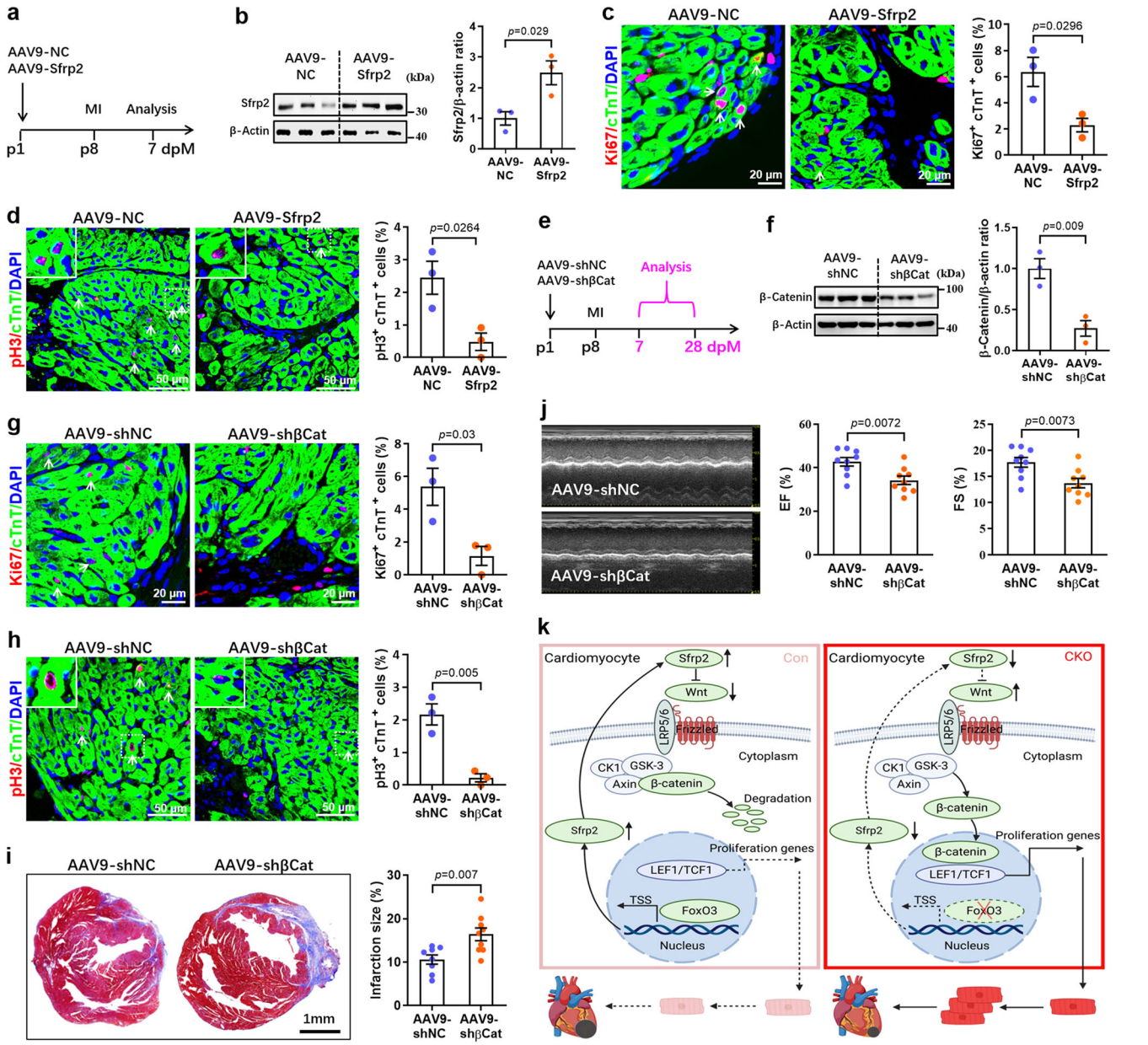

Fig. 9 | Disturbance of endogenous Sfrp2 and β-catenin attenuates cardiomyocyte proliferation in CKO mice. a Schematic of Sfrp2 overexpression, MI induction, and histological analysis in CKO hearts. **b** Western blotting validation of Sfrp2 overexpression in CKO hearts at p8 ($n = 3$ hearts). **c**, **d** Representative images (left) and quantification (right) of Ki67$^+$ (**c**) and pH3$^+$ (**d**) cardiomyocytes in the border zone of infarcted hearts at 7 dpM ($n = 3$ hearts). **e** Schematic of β-catenin knockdown, MI induction, and histological analysis in CKO hearts. **f** Western blotting validation of β-catenin knockdown in CKO hearts at p8 ($n = 3$ hearts). **g**, **h** Representative images (left) and quantification (right) of Ki67$^+$ (**g**) and pH3$^+$ (**h**) cardiomyocytes in the border zone of infarcted hearts at 7 dpM ($n = 3$ hearts). **i** Representative Masson's trichrome staining images (left) and quantification of scar size (right) at 28 dpM ($n = 8$ mice for shNC and 9 mice for shβCat). **j** Representative images of M-model echocardiography (left) and quantification (right) of LVEF and LVFS levels at 28 dpM ($n = 9$ mice). **k** The general view of how FoxO3 controls cardiomyocyte proliferation and heart regeneration through regulating Sfrp2 expression and β-catenin activation. The graphic was created using BioRender.com. All data are presented as the mean ± SEM. *P* values are from two-tailed *t* test (**b**–**d**, **f**–**j**). Source data are provided as a Source Data file.

inhibits cell proliferation in different cell types. A previous study has reported that FoxO1 and FoxO3 are expressed in the developing myocardium concomitant with increased cyclin kinase inhibitor expression from embryonic to neonatal stages[18]. Moreover, it has been reported that FGF10 knockout inhibits cardiomyocyte proliferation via upregulation of p27 through reducing FoxO3 phosphorylation[41]. The proliferation of lung fibroblasts was significantly suppressed by the treatment of UCN-01 (7-hydroxystaurosporine), a FoxO3 activator which can inhibit the phosphorylation and translocation of FoxO3[42].

Using RNA-seq, we identified Sfrp2 as one of downstream targets of FoxO3 during heart injury and regeneration. This finding was further verified by ChIP-qPCR and luciferase reporter gene assays. Mechanistically, our data demonstrate that FoxO3 inhibits canonical Wnt/β-catenin signaling in cardiomyocytes by controlling the expression of Sfrp2 (Figs. 6–8, and Supplementary Figs. 17–19). It is well known that the secreted frizzled-related protein 2 (Sfrp2), a canonical Wnt inhibitor, can compete with Fzd receptor for Wnt binding and prevent the activation of canonical Wnt/β-catenin pathway[43]. Previous study has demonstrated that Sfrp2 inhibits the proliferation of cardiac progenitor cells by binding to Wnt6 and suppressing Wnt/β-catenin canonical pathway[44]. In consistent with this report, we found that Sfrp2 knockdown promotes the proliferation of primary cardiomyocytes

isolated from neonatal mice (Supplementary Fig. 17). Moreover, FoxO3 knockout specifically in cardiomyocytes led to Sfrp2 downregulation (Supplementary Fig. 18). In addition, Sfrp2 overexpression inhibits cardiomyocyte proliferation and heart regeneration in the FoxO3-deficient mice model (Figs. 6 and 7). These findings indicate that FoxO3 negatively regulates cardiomyocyte proliferation and heart regeneration in postnatal mice at least in part by controlling Sfrp2 expression. In contrast with our observation, it has been reported that the Sfrp2 released by the Akt-MSC mediates myocardial survival and repair after ischemic injury in rats[45]. They found that the conditioned medium collected from Akt-MSCs treated with siRNA against Sfrp2 reduces the protection of myocardial injury in vitro and in vivo when compared with those of untreated Akt-MSC-conditioned medium[45]. Moreover, the same group also revealed that exogenously administered Sfrp2 reduces fibrosis and improves cardiac function in a rat model of myocardial infarction[46]. They showed that Sfrp2 can inhibit procollagen maturation in cardiac fibroblasts by suppressing Bmp1 activity[46]. These previous reports suggest that exogenous Sfrp2 may be beneficial for repairing the damaged heart. For the discrepancies between our paper and theirs, there are several possible reasons. First, the experimental conditions are very different between our study and theirs. They revealed the importance of Sfrp2 as a major mediator of Akt-MSCs-mediated paracrine protection and as an inhibitor of procollagen maturation in cardiac fibroblasts, whereas our study showed the involvement of Sfrp2 in FoxO3-mediated cardiomyocyte proliferation and regeneration. Second, they examined the effects of exogenous Sfrp2 on cardiac function, while we revealed the functional importance of endogenous Sfrp2 in cardiomyocytes. Third, they used a rat model, while a mouse model was used in our study. In fact, the important roles of Sfrp2 in heart have been proposed in several previous studies. It has been reported that Sfrp2 inhibits cardiomyogenic differentiation of murine embryonic stem cells by suppressing Wnt3a transcription as well as β-catenin activity[47]. In contrast, a recent study reported that Sfrp2 can switch the fate of multipotent cKit$^+$ cells which typically differentiate into endothelial cells but not cardiomyocytes, and promote their differentiation into cardiomyocytes[48]. These previous studies suggest that the function of Sfrp2 in heart may be pleiotropic under different conditions.

In mammals, the Wnt family of ligands consists of 19 glycoproteins that can be classified into two main modes: the canonical pathway, which prevents the degradation of β-catenin and allows β-catenin-dependent transcriptional regulation to occur, and the non-canonical pathway, which involves β-catenin-independent downstream signaling and can be broadly divided into the planar cell polarity (PCP) pathway and the Ca^{2+}-dependent pathway[49–51]. We found that FoxO3 knockout has no significant impacts on the phosphorylation of JNK and CaMKII (Supplementary Fig. 21a, b), indicating that non-canonical Wnt signaling might be not involved in the phenotypes mediated by FoxO3-Sfrp2 axis in cardiomyocytes. Wnt/β-catenin signaling plays important roles during heart development and its activation is increased in response to cardiac injury in vertebrates[52]. It has been demonstrated that Wnt/β-catenin pathway activation by 6-bromoindirubin-3′-oxime (BIO), a specific pharmacological inhibitor of glycogen synthase kinase-3 (GSK-3), promotes the proliferation of neonatal mammalian cardiomyocytes in vitro[53] and improves cardiac function in vivo[54]. Moreover, inhibition of GSK3β results in nuclear translocation and activation of β-catenin, thereby promoting cardiomyocyte proliferation and cardiac repair in mice and zebrafish[55]. In agreement with these previous studies, our data showed that in vitro and in vivo deficiency of FoxO3 suppressed Sfrp2 and promotes β-catenin expressions in cardiomyocytes (Fig. 8a–d), which was accompanied by the increased activation of β-catenin as demonstrated by TOP/FOP Flash reporter assay (Fig. 8e). Moreover, Sfrp2 overexpression can inhibit β-catenin expression and its activation in FoxO3-deficient cardiomyocytes (Fig. 8i, j). Importantly, interfering with the downregulated Sfrp2 and increased β-catenin in CKO hearts can significantly blocked the cardiomyocyte proliferation induced by FoxO3 knockout at non-regenerative stage (Fig. 9b–h). These findings indicate that FoxO3 deletion enhanced cardiomyocyte proliferation and heart regeneration in neonatal mice, at least in part, through downregulating Sfrp2 expression and subsequently activating canonical Wnt/β-catenin signaling. Although we did not determine the direct binding between Sfrp2 and Wnt ligands, our data revealed that β-catenin is one of effector of FoxO3-Sfrp2 axis-mediated cardiomyocyte proliferation and heart regeneration. Importantly, the prediction data (Supplementary Fig. 21e) and Sfrp2-mediated Wnt8a production (Supplementary Fig. 21f, g) suggest that the canonical Wnt8a/β-catenin may contribute to the phenotypes induced by FoxO3-Sfrp2 axis under our experimental conditions. In fact, functional interaction between β-catenin and FoxO3 has been demonstrated in mammalian cells and in *Caenorhabditis elegans* response to stress[56]. Moreover, deletion of FoxO members including FoxO3 increases proliferation of osteoprogenitor cells and bone formation by upregulating Wnt/β-catenin pathway[57].

In summary, our data show that FoxO3 activity is decreased during postnatal heart regeneration upon injury, which is correlated with an increase in cardiomyocyte proliferation as well as decrease of negative regulators of proliferation and cell cycle. Using loss-of-function genetic experiments in mice, we demonstrate that FoxO3 knockout promotes cardiomyocyte proliferation and heart regeneration in postnatal mice, at least in part, through downregulating Sfrp2 and subsequently activating the canonical Wnt/β-catenin signaling (Fig. 9k). Our data suggest that FoxO3 is a key regulator of cardiomyocyte proliferation, which is sufficient to control the cardiac regeneration in postnatal mice. A deeper understanding of the mechanism by which FoxO3 regulates cardiomyocyte proliferation and cardiac regeneration may provide novel insights into elucidating the molecular mechanism of cardiac damage and repair.

Methods

Cell culture

HL-1 cardiomyocyte cell line (mouse) was obtained from Sigma-Aldrich (USA). HL-1 cells were cultured in Claycomb media (Sigma-Aldrich, USA) supplemented with 10% fetal bovine serum (Gibco, USA), 100 μM norepinephrine (Sigma-Aldrich, USA), 2 mM glutamine (Gibco, USA), 5 units/mL penicillin and 5 μg/mL streptomycin (Gibco, USA), at 37 °C in a 5% CO_2 incubator. Culture medium was replaced every 2 days and cells were passaged when they reached 80% confluence. Cells were mycoplasma negative through treatment with LookOut® Mycoplasma Elimination Kit (Sigma-Aldrich). Gene silencing was achieved by transfecting predesigned siRNA duplexes (Supplementary Table 9) designed and synthesized by RiboBio (Guangzhou, China).

Establishment of stable FoxO3 knockdown cells

The shRNA-expressing lentiviral vector pLOX-U6-Puro[58] was used to establish the stable FoxO3 knockdown cells. Stable knockdown of FoxO3 gene in HL-1 cells was achieved by short-hairpin RNA (shRNA) delivery using lentivirus. FoxO3 specific shRNA or negative control were cloned into pLOX-U6-Puro vectors[22]. Lentiviral vectors and packaging vectors (pCMVR8.74 (#22036) and pMD2.G (#12259), Addgene) were co-transfected into HEK 293T cells using the LipoFiterTM Liposomal Transfection Reagent (Hanbio Biotechnology, Shanghai, China) to generate viruses. The viral supernatant was concentrated with the Lenti Virus Concentration Reagent (Biomiga, CA, USA) and used to infect HL-1 cells. Infected HL-1 cells were selected by puromycin and expanded to form a stable sub-line. Knockdown efficiency was confirmed at both mRNA and protein levels. Stable cell line generated by FoxO3-shRNA and negative shRNA were named as shFoxO3 cells and shNC cells, respectively.

Overexpression vector construction

Total RNA was isolated using RNeasy kit (Qiagen, Valencia, CA, USA) from HL-1 cells according to the manufacture's instruction. The cDNA was transcribed from total RNA using SuperScript III Reverse Transcriptase (Roche, USA). The coding sequence (CDS) of FoxO3 (NM_015760.5) ware amplified by the KOD-Plus-Neo Kit (Toyobo, Japan) and cloned into the pcDNA3.1 expression vector to construct the pcDNA-FoxO3 plasmid. Constructed overexpression plasmid pcDNA-FoxO3 was used to explore the effect of FoxO3 on luciferase reporter gene as below described.

Adeno-associated virus 9 (AAV9) and adenovirus type 5 (Adv5) production

The full-length CDS of Sfrp2 (NM_009144.2) was amplified using the cDNA template from HL-1 cells as above described. The amplified Sfrp2 cDNA sequence was cloned into AAV9- and Adv5-expressing plasmids driving by the cardiomyocyte-specific cTnT promoter to package and generate AAV9-cTnT-Sfrp2 (AAV9-Sfrp2) and Adv5-cTnT-Sfrp2 (Adv5-Sfrp2) viruses (DongBio.Co.Ltd, Shenzhen, China), respectively. Viruses packaged with empty plasmids (AAV9-NC and Adv5-NC) served as negative controls for AAV9-Sfrp2 and Adv5-Sfrp2, respectively. To overexpress Sfrp2 specifically in myocardium in vivo, AAV9 virus was subcutaneously injected into neonatal mice at postnatal day 1 (p1) at a dose of 5×10^{10} V.G./mouse. To overexpress Sfrp2 in vitro, primary cardiomyocytes and HL-1 cells were infected with Adv5 virus (1×10^{10} PFU/mL) at a multiplicity of infection (MOI) of 50.

Animals

All animal experiments were performed in accordance with institutional guidelines and with the approval of the Institutional Animal Care and Use Committee of Jinan University (IACUC-20210611-03). Mice were housed in a specific pathogen-free (SPF) animal facility at Jinan University under a 12-h light/dark cycle, a temperature range of 25 ± 1 °C, and a humidity of 50 ± 5%. Animal health was monitored according to the Association for Assessment and Accreditation of Laboratory Animal Care (AAALAC) guidelines. FoxO3-LoxP-targeted ($FoxO3^{fl/fl}$) mice (C57BL/6 background)[21,22] were created by Cyagen Biosciences (Suzhou, China). The exon 3 region of the FoxO3 gene was flanked by LoxP sites and deleted upon Cre-mediated recombination (Fig. S3A). $FoxO3^{fl/fl}$ mice and Myh6-Cre transgenic line (Jackson Laboratory, stock number 011038) were genotyped using specific PCR primers including FoxO3fl-Forward (5'-CAG CCG GTT CAT CAG AGT TTT ACC-3'), FoxO3fl-Reverse (5'-CTA TCA ACG AGG TAG TGA TCT AAG AAC ATG C-3'), 9543 (5'-ATG ACA GAC AGA TCC CTC CTA TCT CC-3'), and 9544 (5'-CTC ATC ACT CGT TGC ATC ATC GAC-3')[21]. The $FoxO3^{fl/fl}$ mice were crossed with Myh6-Cre mice to generate $FoxO3^{fl/fl}$::Myh6-Cre mice (CKO) with cardiomyocyte-specific knockout of FoxO3. Age-matched Myh6-Cre mice with normal expression of FoxO3 were used as control mice (Con).

Apical resection surgeries were performed on neonatal mice at postnatal day 1 (p1) or p8, followed by heart collection at indicated time points. In brief, neonatal mice were anesthetized by cooling on an ice bed for 4 min. Lateral thoracotomy was then performed by blunt dissection of the intercostal muscles following skin incision. After exposing the left ventricular chamber, iridectomy scissors were used to resect the apex of neonatal hearts. Following apical resection, neonates were removed from the ice bed, thoracic wall incisions were sutured with 7-0 non-absorbable silk suture, and the skin wound closed using skin adhesive. Sham-operated mice underwent the same procedure without apical resection. Neonates were then placed under a heat lamp and warmed for several minutes until recovery. In addition, myocardium infarction (MI) injury in postnatal (p8) and adult mice (2-month-old) was also induced by permanent ligation of the left anterior descending artery (LAD). In brief, p8 and adult mice were anesthetized by cooling and pentobarbital sodium (i.p., 90 mg/kg, Sigma-Aldridge), respectively. The left thoracic region was then shaved and sterilized. The heart was exposed through a left thoracotomy after intubation. The LAD was permanently ligated using a suture. The thoracotomy and skin were then sutured closed in layers. After removal of the excess air from the thoracic cavity, the mouse was removed from ventilation when normal breathing was established. At indicated time points after surgery, the anesthetized mice were then euthanized by cervical dislocation, and the hearts were extracted for detection of various indicators. Moreover, $FoxO3^{fl/fl}$ mice were also crossbred with inducible cardiomyocyte-specific Cre mice ($Myh6^{MCM}$) to generate $FoxO3^{fl/fl}$::$Myh6^{MCM}$ mice (iCKO), of which the cardiomyocyte-specific knockout of FoxO3 could be induced by tamoxifen administration at the indicated time points. Adult (8-week-old) iCKO mice were injected with tamoxifen (50 mg/kg, i.p.) for 5 days to induce the cardiomyocyte-specific knockout of FoxO3, followed by the permanent ligation of the left anterior descending artery (LAD) to induce myocardium infarction (MI) injury. Both male and female C57BL/6J mice were used for neonatal heart injury experiments. For experiments using adult animals, male mice were used in this study. All animals were randomly distributed into different groups according to the detailed animal experiments.

Echocardiograph

Animals with or without heart injury were anesthetized with 1–2% isoflurane and subjected to echocardiography analysis at indicated time points. Cardiac function was evaluated using the Vevo® 2100 ultrasound system (Visualsonics, Toronto, Canada) equipped with a high-frequency (30 MHz) linear array transducer. Parasternal long-axis, short-axis, and two apical four-chamber views were used to obtain 2-dimensional and M-mode images. The ejection fraction (EF) and fractional shortening (FS) were calculated by the Vevo® 2100 ultrasound system automatically.

Primary cardiomyocytes isolation, nucleation, and transfection

To isolate primary cardiomyocytes, fresh mice hearts were harvested and immediately fixed in 4% PFA/PBS at 4 °C for 4 h. The whole hearts were subsequently incubated with collagenase IV (2.4 mg/ml, Sigma) and II (1.8 mg/ml, Sigma) for 12 h at 37 °C. The supernatant was collected and spun down in 500 rpm for 2 min to yield the cardiomyocytes. The remaining hearts were then minced to smaller pieces and the procedure was repeated until no more cardiomyocytes were dissociated from the hearts. The cardiomyocytes were stained with DAPI for nucleation counts. For nucleation, a total of about 1000 cardiomyocytes were counted per heart. Knockdown and overexpression of target genes in primary cardiomyocytes were induced by siRNAs transfection and Adv5-mediated expression, respectively. For cardiomyocytes count, we averaged 2 different counts/sample and 3–6 hearts/group using a hemocytometer.

Histology

Mice were sacrificed and weighed to obtain total body weight (BW) at indicated time points. The heart was then harvested and weighed to obtain heart weight (HW) and HW/BW ratio. Harvested hearts were fixed in 4% paraformaldehyde (PFA)/PBS solution overnight at room temperature, dehydrated in an ethanol series, and then processed for paraffin embedding. Paraffin sections were cut in 5 μm thickness. Sections were subjected to Masson's trichrome and Hematoxylin/eosin (H&E) staining according to standard procedures. Fibrotic scar size was measured using the CaseViewer version 2.1 software (3DHISTECH, Hungary). The whole images of hearts were captured by Leica M205FA stereo fluorescence microscope to visualize the apex regeneration at indicated time points.

Immunofluorescence staining

Hearts were embedded in paraffin and cut in 5 μm sections, deparaffinized, rehydrated, and antigen retrieval. Sections were permeabilized

with 0.5% Triton X-100/PBS and then blocked with 5% goat serum (Jackson ImmunoResearch Laboratories, USA) for 1 h at room temperature, and incubated with primary antibodies overnight at 4 °C. After washing with PBS, sections were incubated with corresponding secondary antibodies conjugated to fluorescence for 1 h at room temperature, followed by counterstaining with DAPI (Sigma). Primary antibodies are follows: anti-FoxO3 (CST, #2497, 1:200), anti-Ki67 (Abcam, ab16667, 1:250), anti-phospho-Histone H3 (pH3) (CST, #53348S, 1:400), anti-aurora kinase B (AurkB) (Abcam, ab2254, 1:200), and anti-Cardiac Troponin T (cTnT) (ThermoFisher, MA512960, 1:200). Secondary antibodies used are following: Alexa Fluor 488 goat anti-mouse IgG (Jackson ImmunoLabs, 115-545-071, 1:200), Alexa Fluor 488 goat anti-rabbit IgG (Jackson ImmunoLabs, 111-545-003, 1:200), Cy3-conjugated Affinipure Goat anti-mouse IgG (Proteintech, SA00009-1, 1:200); Cy3-conjugated Affinipure Goat anti-Rabbit IgG (Proteintech, SA00009-2, 1:200). The slides were imaged with fluorescence microscope (Leica Microsystems) or Zeiss LSM 700 laser confocal microscope (Carl Zeiss).

Wheat germ agglutinin (WGA) staining

Following deparaffinized, rehydrated, slides were then incubated with WGA conjugated to Alexa Fluor 488 (Invitrogen, W11261, 5 µg/ml) for 10 min at room temperature. To quantify the cell size, 5 independent hearts per group (at least 300 cells) were captured near apex with laser-scanning confocal microscope (LSM 700, Zeiss). ZEN 2012 lite software (Zeiss) was used to quantify the size of each cell.

EdU labeling assay in vivo

For EdU labeling experiments, neonatal mice were subcutaneously injected with 50 µl of a 2 mg/ml solution of EdU (RiboBio, Guangzhou, China) dissolved in sterile water. Hearts were embedded in Tissue-Tek optimal cutting temperature compound (OCT) (Sakura, USA) for frozen section (4 µm). Sections were rinsed three times in PBS and fixed in 4% parapormaldehyde for 30 min. After rinsing three times again, citrate antigen retrieval was performed as described above. Sections were then incubated with 2 mg/mL glycine solution for 10 min, permeabilized with 0.5% Triton X-100 in PBS for 10 min, and then rinsed with PBS once for 5 min. This was followed by incubation with Apollo®576 staining solution (1×) at room temperature for 30 min. Permeabilization was performed again with 0.5% Triton X-100 in PBS twice for 10 min. Sections were then rinsed with methanol for 5 min, washed with PBS once for 5 min, blocked with 5% goat serum for 1 h, and followed by incubation with primary antibody against cTnT (ThermoFisher, MA512960, 1:200) overnight. The following day, incubation with anti-mouse secondary antibody conjugated to Alexa Fluor 488 (1:200 dilution, Jackson ImmunoResearch Laboratories, USA) was performed. Sections were washed three times in PBS, stained with DAPI for 10 min to label nuclei, and mounted in Antifade Mounting Medium. Images were captured by laser-scanning confocal microscope (LSM 700, Zeiss) and analyzed by ZEN 2012 software (Zeiss).

To analyze CMs proliferation at the indicated time points, EdU was injected 8 h prior to heart collection. For EdU pulse-chase experiments, EdU was injected once every two days to label all proliferating CMs during the whole period of cardiac regeneration. The last injection was performed 8 h prior to heart collection. Sham-operated mice underwent the same procedure without the apical resection.

In vitro cell proliferation assay

For cell proliferation assay, both primary cardiomyocytes and HL-1 cell line were incubated in 24-well plates with different treatments. DNA synthesis were then analyzed by EdU labeling, using Cell-Light™ EdU Apollo®567 In Vitro Imaging Kit (RiboBio, Guangzhou, China) according to the manufacturer's instructions. At least 5 images were randomly taken per well using a Zeiss LSM 700 laser confocal microscope (Carl Zeiss). The population of EdU^+ cells was determined by counting at least 500 cells per well. The EdU^+ cells were quantified as the percentage of total cells. HL-1 cell proliferation was also analyzed using the Enhanced Cell Counting Kit-8 (CCK-8, Beyotime Biotechnology, China) according to the manufacturer's instructions. Moreover, proliferation of primary cardiomyocytes was also performed by Ki67, pH3, and AukrB staining together with cTnT staining.

RNA-sequencing

For total RNA isolation, hearts were extracted in control and FoxO3 CKO mice at p1 and p14, respectively. Three ventricles per group were used for RNA-sequencing analysis. RNA was isolated from the ventricles using TRIzol™ Reagent (Invitrogen), followed by reverse transcription using random primers to obtain cDNA library for sequencing on GBISEQ-500 platform. After filtering the reads with low quality, clean reads were then obtained and mapped to the reference genome of mouse (GRCm38.p6) with HISAT[59]. Genes expression level was quantified by a software package called RSEM[60] and expressed as fragments per kilobase of exon per million fragments mapped (FPKM). Differential expressed (DE) genes were detected using NOISeq method[61] with Probability ≥ 0.8 and fold change (FC) of FPKM ≥ 2. Only those genes were considered for the differential expression analysis, which displayed FPKM ≥ 1 in either of the two samples under comparison. GO analysis was performed using online tool DAVID 6.8 (https://david.ncifcrf.gov/summary.jsp), and terms with p-value ≤ 0.05 were included. Differentially expressed gene heat maps were clustered by hierarchical clustering using cluster software[62]. Gene set enrichment analysis (GSEA) was performed to identify gene sets from signaling pathways that showed statistical differences between two groups by using GSEA software (http://software.broadinstitute.org/gsea/index.jsp).

RNA extraction and quantitative real-time PCR (qPCR)

Total RNA was isolated using RNeasy Kit (Qiagen, Valencia, CA, USA) from cells or heart tissue according to the protocol of the manufacturer, respectively. Reverse transcription to cDNA was performed with 30 ng of total RNA, random primers, and SuperScript III Reverse Transcriptase (Roche, USA). The qPCR was performed using a Light Cycler 480 SYBR Green I Master (Roche, USA) and the MiniOpticon qPCR System (Bio-Rad, CA, USA). After denaturation for 10 min at 95 °C, the reactions were subjected to 45 cycles of 95 °C for 30 s, 60 °C for 30 s, and 72 °C for 30 s. GAPDH was used as the internal standard control to normalize gene expression using the 2-ΔΔCt method. The sequences of the qPCR primers were listed in Supplementary Table 10.

Protein extracts and Western blotting

Tissue for SDS-PAGE was lysed in RIPA buffer (Beyotime Biotechnology) containing protease inhibitors (Sigma). Protein concentration ware determined using the Bio-Rad Protein Assay (Bio-Rad Laboratories). 30 µg of protein were separated by SDA-PAGE, proteins were transferred onto PVDF membranes (Millipore), then blocked in 5% nonfat milk/TBS-Tween 20 and incubated with primary antibodies (dilution in TBST) overnight at 4 °C. Membranes were then washed and incubated with corresponding second antibodies for 1 h at room temperature. Bands were detected by chemiluminescence reagents (ThermoFisher Scientific). Primary antibodies used are following: anti-FoxO3 (CST, #2497), anti-phospho-FoxO3 (T32) (Abcam, ab26649), anti-phospho-FoxO3 (Ser253) (CST, #9466), anti-Akt (CST, #9272), anti-phospho-Akt (CST, #4060), anti-Sfrp2 (Abcam, ab137560), anti-β-catenin (Abcam, ab32572), anti-β-actin (Proteintech, 60008-1-Ig), anti JNK (HUABIO, ET1601-28), anti-phospho-JNK (HUABIO, ET1609-42), anti-CaMKII (HUABIO, ET1608-47), anti-phospho-CaMKII (HUABIO, HA721794), anti-Wnt1 (Proteintech, 27935-1-AP), anti-Wnt2b (HUABIO, ET7107-20), anti-Wnt4 (Biodragon, BD-PN0285), anti-Wnt8a

(Biodragon, BD-PN0289), anti-Wnt10b (Proteintech, 67210-1-Ig). Secondary antibodies used are the following: goat-anti-mouse horseradish peroxidase (HRP)-conjugated antibody (CST, #7076); goat-anti-rabbit horseradish peroxidase (HRP)-conjugated antibody (CST, #7074). Quantitation of the chemiluminescent signal was analyzed using Image-Pro Plus version 6.0 (Media Cybernetics, Bethesda, MD). The relative expression levels of target protein/β-actin ratio was set as one in control group. All blots derive from the same experiment and were processed in parallel.

Chromatin immunoprecipitation (ChIP)-qPCR assay

The promoter sequences (−2000 bp to −1 bp, upstream of TSS) of the mouse genes including Trp53 (Gene ID: 22059), Sfrp2 (Gene ID: 20319), Cdkn2c (Gene ID: 12580), and Cdkn2d (Gene ID: 791073) were analyzed by JASPAR 2022 online software (http://jaspar.genereg.net/)[63] to determine potential FoxO3 binding sites (Supplementary Tables 3–6). The predicted binding site with highest score for each promoter was further analyzed by ChIP-qPCR assay, to evaluate the in vivo binding of FoxO3 to its consensus sequence in mouse target gene promoters using heart tissues. The assays were performed using the SimpleChIP® Plus Enzymatic Chromatin IP Kit (CST, #9004) according to the manufacturer's protocol. FoxO3 antibody (CST, #2497) was used to immunoprecipitation assay. Normal goat IgG (CST, #2729) was used as a control as previously described. The DNA isolated from input chromatin fragments by IgG and from the precipitated chromatin fragments by anti-FoxO3 antibody were subjected to qPCR using specific primers (Supplementary Table 11) flanking the consensus FoxO3 binding sites on target promoters. Relative binding ability of FoxO3 was expressed as the DNA signals relative to input.

Dual-luciferase reporter assay

The dual-luciferase reporter plasmid (pGR)[22] consists of the Gaussia luciferase (GL) driven by CMV promoter and the Red Firefly luciferase (RF) driven by HSV-TK promoter. The predicted FoxO3 binding sites with highest score for target gene promoters were further analyzed by pGR dual-luciferase reporter assay, to evaluate the in vitro binding and regulating effects of FoxO3 on target genes. Briefly, promoter regions of target genes comprising predicted FoxO3 binding sites were amplified and cloned into the upstream of GL in pGR plasmid to replace CMV promoter, thereby constructing pTrp53-GR and pSfrp2-GR dual-luciferase reporter plasmids. For pTrp53-GR plasmid construction, a 614-bp DNA fragment (−744 to −127 upstream of TSS) comprising the predicted FoxO3 binding sites (top2) in the promoter region of Trp53 was amplified and cloned into pGR plasmid. Regarding the pSfrp2-GR plasmid construction, a 751-bp DNA fragment (−1989 to −1239 upstream of TSS) comprising the predicted FoxO3 binding site with highest score in the promoter region of Sfrp2 was used. HL-1 cells were co-transfected with the dual-luciferase reporter plasmids and pcDNA-FoxO3 plasmid (50 ng for each plasmid) for 48 h using Lipo-Fiter Liposomal Transfection Reagent (Hanbio Biotechnology). Luciferase reporter assay was then carried out using the Pierce™ Gaussia-Firefly Luciferase Dual Assay Kit (ThermoFisher Scientific) according to the manufacturer's protocol. Luciferase activity was measured using a BioTek Synergy™ 4 multimode microplate reader (BioTek Instruments). The relative activity of the Gaussia luciferase was normalized by the activity of Red Firefly luciferase and was expressed as fold change of control group. To further verify the potential binding sites, mutant luciferase reporter plasmids were generated by KOD-Plus-Mutagenesis Kit (Toyobo, Osaka, Japan), according to the manufacturer's protocol. To examine the activity of β-catenin, TOP-Flash reporter assay was performed. In brief, HL-1 cells were co-transfected with constant quantities of reporter plasmids expressing Red Firefly luciferase (TOP-Flash, specific for β-catenin; Addgene, #12456) and pTK-*Gaussia* Luc reporter plasmid (indicator of the transfection efficiency; ThermoFisher). Dual-luciferase assay was performed using the Pierce™ Gaussia-Firefly Luciferase Dual Assay Kit (ThermoFisher Scientific) according to the manufacturer's protocol. The Red Firefly luciferase (RF) activity was normalized to the corresponding *Gaussia* luciferase (GL) activity and was expressed as fold change of control group.

Statistical analysis

All statistics were calculated using GraphPad Prism 8 Software. Among three or more groups, statistical analysis was performed using one-way ANOVA with Tukey's multiple comparisons test or two-way ANOVA with Sidak's multiple comparisons test. Comparisons between two groups were analyzed using unpaired and two-tailed Student's *t* test. All data are presented as the mean ± SEM. A p value less than 0.05 was considered statistically significant. In this study, statistical analysis was in accordance with homogeneity of variance and normality of residuals. Homogeneity of variance was evaluated by the F test with a p value of greater than 0.05. Normality of residuals was evaluated by D'Agostino-Pearson test and/or Shapiro–Wilk test with a p value of more than 0.05.

Reporting summary

Further information on research design is available in the Nature Portfolio Reporting Summary linked to this article.

Data availability

All the RNA-seq data are available from NCBI Sequence Read Archive (BioProject accession: PRJNA951351). Other data generated in this study are provided in the Supplementary Information and Source data files. Source data are provided with this paper.

References

1. Bergmann, O. et al. Evidence for cardiomyocyte renewal in humans. *Science* **324**, 98–102 (2009).
2. Hsieh, P. C. H. et al. Evidence from a genetic fate-mapping study that stem cells refresh adult mammalian cardiomyocytes after injury. *Nat. Med.* **13**, 970–974 (2007).
3. Pasumarthi, K. B. S., Nakajima, H., Nakajima, H. O., Soonpaa, M. H. & Field, L. J. Targeted expression of cyclin D2 results in cardiomyocyte DNA synthesis and infarct regression in transgenic mice. *Circ. Res.* **96**, 110–118 (2005).
4. Senyo, S. E. et al. Mammalian heart renewal by pre-existing cardiomyocytes. *Nature* **493**, 433–436 (2013).
5. Laflamme, M. A. & Murry, C. E. Regenerating the heart. *Nat. Biotechnol.* **23**, 845–856 (2005).
6. D'Uva, G. et al. ERBB2 triggers mammalian heart regeneration by promoting cardiomyocyte dedifferentiation and proliferation. *Nat. Cell Biol.* **17**, 627–638 (2015).
7. Li, F., Wang, X., Capasso, J. M. & Gerdes, A. M. Rapid transition of cardiac myocytes from hyperplasia to hypertrophy during postnatal development. *J. Mol. Cell Cardiol.* **28**, 1737–1746 (1996).
8. Soonpaa, M. H. & Field, L. J. Survey of studies examining mammalian cardiomyocyte DNA synthesis. *Circ. Res.* **83**, 15–26 (1998).
9. Poss, K. D., Wilson, L. G. & Keating, M. T. Heart regeneration in zebrafish. *Science* **298**, 2188–2190 (2002).
10. Jopling, C. et al. Zebrafish heart regeneration occurs by cardiomyocyte dedifferentiation and proliferation. *Nature* **464**, 606–U168 (2010).
11. Liao, S. et al. Heart regeneration in adult Xenopus tropicalis after apical resection. *Cell Biosci.* **7**, 70 (2017).
12. Wu, H. Y. et al. Fosl1 is vital to heart regeneration upon apex resection in adult Xenopus tropicalis. *NPJ Regen. Med.* **6**, 36 (2021).
13. Porrello, E. R. et al. Transient Regenerative Potential of the Neonatal Mouse Heart. *Science* **331**, 1078–1080 (2011).
14. Porrello, E. R. et al. Regulation of neonatal and adult mammalian heart regeneration by the miR-15 family. *Proc. Natl Acad. Sci. USA* **110**, 187–192 (2013).

15. Mahmoud, A. I. et al. Meis1 regulates postnatal cardiomyocyte cell cycle arrest. *Nature* **497**, 249–253 (2013).
16. Jiang, F. Q. et al. Mettl3-mediated m(6)A modification of Fgf16 restricts cardiomyocyte proliferation during heart regeneration. *Elife* **11**, e77014 (2022).
17. Becker, R. O., Chapin, S. & Sherry, R. Regeneration of the ventricular myocardium in amphibians. *Nature* **248**, 145–147 (1974).
18. Evans-Anderson, H. J., Alfieri, C. M. & Yutzey, K. E. Regulation of cardiomyocyte proliferation and myocardial growth during development by FOXO transcription factors. *Circ. Res.* **102**, 686–694 (2008).
19. Shimokawa, I. et al. The life-extending effect of dietary restriction requires Foxo3 in mice. *Aging Cell* **14**, 707–709 (2015).
20. Tsuchiya, K. et al. FoxOs integrate pleiotropic actions of insulin in vascular endothelium to protect mice from atherosclerosis. *Cell Metab.* **15**, 372–381 (2012).
21. Chang, Z. S. et al. Forkhead box O3 protects the heart against paraquat-induced aging-associated phenotypes by upregulating the expression of antioxidant enzymes. *Aging Cell* **18**, e12990 (2019).
22. Liang, C. Q. et al. FoxO3 restricts liver regeneration by suppressing the proliferation of hepatocytes. *NPJ Regen. Med.* **7**, 33 (2022).
23. Hosaka, T. et al. Disruption of forkhead transcription factor (FOXO) family members in mice reveals their functional diversification. *Proc. Natl Acad. Sci. USA* **101**, 2975–2980 (2004).
24. Sengupta, A., Molkentin, J. D., Paik, J. H., DePinho, R. A. & Yutzey, K. E. FoxO transcription factors promote cardiomyocyte survival upon induction of oxidative stress. *J. Biol. Chem.* **286**, 7468–7478 (2011).
25. Hannenhalli, S. et al. Transcriptional genomics associates FOX transcription factors with human heart failure. *Circulation* **114**, 1269–1276 (2006).
26. Ni, Y. G. et al. Foxo transcription factors blunt cardiac hypertrophy by inhibiting calcineurin signaling. *Circulation* **114**, 1159–1168 (2006).
27. Schips, T. G. et al. FoxO3 induces reversible cardiac atrophy and autophagy in a transgenic mouse model. *Cardiovasc. Res.* **91**, 587–597 (2011).
28. Galasso, G. et al. Myocardial expression of FOXO3a-Atrogin-1 pathway in human heart failure. *Eur. J. Heart Fail* **12**, 1290–1296 (2010).
29. Brunet, A. et al. Akt promotes cell survival by phosphorylating and inhibiting a Forkhead transcription factor. *Cell* **96**, 857–868 (1999).
30. Bersell, K., Arab, S., Haring, B. & Kuhn, B. Neuregulin1/ErbB4 signaling induces cardiomyocyte proliferation and repair of heart injury. *Cell* **138**, 257–270 (2009).
31. Hesse, M. et al. Midbody positioning and distance between daughter nuclei enable unequivocal identification of cardiomyocyte cell division in mice. *Circ. Res.* **123**, 1039–1052 (2018).
32. Deogharia, M. et al. Histone demethylase KDM5 regulates cardiomyocyte maturation by promoting fatty acid oxidation, oxidative phosphorylation, and myofibrillar organization. *Cardiovasc. Res.* **120**, 630–643 (2024).
33. Li, X. et al. Inhibition of fatty acid oxidation enables heart regeneration in adult mice. *Nature* **622**, 619–626 (2023).
34. Sengupta, A., Kalinichenko, V. V. & Yutzey, K. E. FoxO1 and FoxM1 transcription factors have antagonistic functions in neonatal cardiomyocyte cell-cycle withdrawal and IGF1 gene regulation. *Circ. Res.* **112**, 267–277 (2013).
35. Zuppo D. A. et al. Foxm1 regulates cardiomyocyte proliferation in adult zebrafish after cardiac injury. *Development* **150**, dev201163 (2023).
36. Akoumianakis, I., Polkinghorne, M. & Antoniades, C. Non-canonical WNT signalling in cardiovascular disease: mechanisms and therapeutic implications. *Nat. Rev. Cardiol.* **19**, 783–797 (2022).
37. Duan, J. et al. Wnt1/betacatenin injury response activates the epicardium and cardiac fibroblasts to promote cardiac repair. *EMBO J.* **31**, 429–442 (2012).
38. Peng, X. et al. Wnt2bb induces cardiomyocyte proliferation in zebrafish hearts via the jnk1/c-jun/creb1 pathway. *Front Cell Dev. Biol.* **8**, 323 (2020).
39. Paik, D. T. et al. Wnt10b gain-of-function improves cardiac repair by arteriole formation and attenuation of fibrosis. *Circ. Res.* **117**, 804–816 (2015).
40. Eijkelenboom, A. & Burgering, B. M. FOXOs: signalling integrators for homeostasis maintenance. *Nat. Rev. Mol. Cell Biol.* **14**, 83–97 (2013).
41. Rochais, F. et al. FGF10 promotes regional foetal cardiomyocyte proliferation and adult cardiomyocyte cell-cycle re-entry. *Cardiovasc. Res.* **104**, 432–442 (2014).
42. Al-Tamari, H. M. et al. FoxO3 an important player in fibrogenesis and therapeutic target for idiopathic pulmonary fibrosis. *EMBO Mol. Med.* **10**, 276–293 (2018).
43. Hsueh, Y. C., Hodgkinson, C. P. & Gomez, J. A. The role of Sfrp and DKK proteins in cardiomyocyte development. *Physiol. Rep.* **9**, e14678 (2021).
44. Schmeckpeper, J. et al. Inhibition of Wnt6 by Sfrp2 regulates adult cardiac progenitor cell differentiation by differential modulation of Wnt pathways. *J. Mol. Cell Cardiol.* **85**, 215–225 (2015).
45. Mirotsou, M. et al. Secreted frizzled related protein 2 (Sfrp2) is the key Akt-mesenchymal stem cell-released paracrine factor mediating myocardial survival and repair. *Proc. Natl Acad. Sci. USA* **104**, 1643–1648 (2007).
46. He, W. et al. Exogenously administered secreted frizzled related protein 2 (Sfrp2) reduces fibrosis and improves cardiac function in a rat model of myocardial infarction. *Proc. Natl Acad. Sci. USA* **107**, 21110–21115 (2010).
47. Deb, A. et al. SFRP2 regulates cardiomyogenic differentiation by inhibiting a positive transcriptional autofeedback loop of Wnt3a. *Stem Cells* **26**, 35–44 (2008).
48. Gomez, J. A., Payne, A., Pratt, R. E., Hodgkinson, C. P. & Dzau, V. J. A role for Sfrp2 in cardiomyogenesis in vivo. *Proc. Natl Acad. Sci. USA* **118**, e2103676118 (2021).
49. Zimmerman, Z. F., Moon, R. T. & Chien, A. J. Targeting Wnt pathways in disease. *Cold Spring Harb. Perspect. Biol.* **4**, a008086 (2012).
50. Marinou, K., Christodoulides, C., Antoniades, C. & Koutsilieris, M. Wnt signaling in cardiovascular physiology. *Trends Endocrinol. Metab.* **23**, 628–636 (2012).
51. Clevers, H. & Nusse, R. Wnt/beta-catenin signaling and disease. *Cell* **149**, 1192–1205 (2012).
52. Ozhan, G. & Weidinger, G. Wnt/beta-catenin signaling in heart regeneration. *Cell Regen.* **4**, 3 (2015).
53. Tseng, A. S., Engel, F. B. & Keating, M. T. The GSK-3 inhibitor BIO promotes proliferation in mammalian cardiomyocytes. *Chem. Biol.* **13**, 957–963 (2006).
54. Lal, H., Ahmad, F., Woodgett, J. & Force, T. The GSK-3 family as therapeutic target for myocardial diseases. *Circ. Res.* **116**, 138–149 (2015).
55. Magadum, A. et al. Live cell screening platform identifies PPAR delta as a regulator of cardiomyocyte proliferation and cardiac repair. *Cell Res.* **27**, 1002–1019 (2017).
56. Essers, M. A. G. et al. Functional interaction between beta-catenin and FOXO in oxidative stress signaling. *Science* **308**, 1181–1184 (2005).
57. Iyer, S. et al. FOXOs attenuate bone formation by suppressing Wnt signaling. *J. Clin. Invest* **123**, 3409–3419 (2013).
58. Qi, X. F. et al. FoxO3a suppresses the senescence of cardiac microvascular endothelial cells by regulating the ROS-mediated cell cycle. *J. Mol. Cell Cardiol.* **81**, 114–126 (2015).

59. Kim, D., Landmead, B. & Salzberg, S. L. HISAT: a fast spliced aligner with low memory requirements. *Nat. Methods* **12**, 357–U121 (2015).
60. Li, B. & Dewey, C. N. RSEM: accurate transcript quantification from RNA-Seq data with or without a reference genome. *BMC Bioinforma.* **12**, 323 (2011).
61. Tarazona, S., Garcia-Alcalde, F., Dopazo, J., Ferrer, A. & Conesa, A. Differential expression in RNA-seq: a matter of depth. *Genome Res.* **21**, 2213–2223 (2011).
62. Eisen, M. B., Spellman, P. T., Brown, P. O. & Botstein, D. Cluster analysis and display of genome-wide expression patterns. *Proc. Natl Acad. Sci. USA* **95**, 14863–14868 (1998).
63. Castro-Mondragon, J. A. et al. JASPAR 2022: the 9th release of the open-access database of transcription factor binding profiles. *Nucleic Acids Res.* **50**, D165–D173 (2022).

Acknowledgements

This work was supported by the grants from the National Natural Science Foundation of China (82030039 to Z.Y.J.), the National Key R&D Program of China (2021YFA1100103 to Z.Y.J.), the National Natural Science Foundation of China (82230047 and 32341004 to Z.Y.J., 82370247, 82070257, and 81770240 to X.F.Q., 82202815 to J.B.X.), the Innovation Team Project of Universities in Guangdong Province (2023KCXTD004 to Z.Y.J.), the Fundamental Research Funds for the Central Universities (21623110 to X.F.Q.), the Open Program of Guangdong Provincial Key Laboratory of Medical Molecular Diagnostics (GPKLMMD-OP202302 to X.F.Q.), the Research Grant of Key Laboratory of Regenerative Medicine of Ministry of Education (ZSYXM202402, ZSYXM202303, ZSYXM202206, and ZSYXM202104 to X.F.Q.), the Guangdong Natural Science Funds for Distinguished Young Scholar (2014A030306011 to X.F.Q.), and the Top Young Talents of Guangdong Province Special Support Program (87315007 to X.F.Q.), China.

Author contributions

J.B.X., K.L., X.L.L., and H.J.L. performed most experiments, and analyzed the data. J.H.L., C.Q.L., Y.C., and N.W. contributed animal and cellular experiments as well as bioinformatic analysis. L.L., Z.F.L., H.Z., K.S.P., and G.H.S. provided valuable comments. Z.Y.J., D.Q.C., and Z.B.Y. revised and edited the manuscript. X.F.Q. conceived of and supervised the study. X.F.Q. wrote the manuscript with help from Z.Y.J., D.Q.C., and Z.B.Y.

Competing interests

The authors declare no competing interests.

Additional information

Supplementary information The online version contains supplementary material available at https://doi.org/10.1038/s41467-025-57962-9.

Correspondence and requests for materials should be addressed to Ze-Bing Ye, Dong-Qing Cai, Zhen-Yu Ju or Xu-Feng Qi.

Peer review information *Nature Communications* thanks Xuejun Yuan, and the other, anonymous, reviewer(s) for their contribution to the peer review of this work. A peer review file is available.